NASA Technical Memorandum 107594

# ACTIVE FLUTTER SUPPRESSION USING "DIPOLE" FILTERS

S. Srinathkumar
Martin R. Waszak

Langley Research Center
Hampton, Virginia

September 1992

NASA
National Aeronautics and
Space Administration

Langley Research Center
Hampton, VA 23665

# ACTIVE FLUTTER SUPPRESSION USING 'DIPOLE' FILTERS

**S. Srinathkumar, Senior NRC Research Associate**
**Martin R. Waszak, Aerospace Engineer**

**NASA Langley Research Center**
**Hampton, Virginia**

## SUMMARY

By using traditional control concepts of gain root locus, the active suppression of a flutter mode of a flexible wing is examined. It is shown that the attraction of the unstable mode towards a critical system zero determines the degree to which the flutter mode can be stabilized. For control situations where the critical zero is adversely placed in the complex plane, a novel compensation scheme called a 'Dipole' filter is proposed. This filter ensures that the flutter mode is stabilized with acceptable control energy. The control strategy is illustrated by designing flutter suppression laws for an active flexible wing (AFW) wind-tunnel model, where minimal control effort solutions are mandated by control rate saturation problems caused by wind-tunnel turbulence.

# INTRODUCTION

Modern aircraft designs emphasize reduction of structural weight to enhance aerodynamic performance. The resulting airframe flexibility often leads to the dynamic aeroelastic instability called flutter. Active control techniques have been extensively investigated to suppress flutter instability and expand the flight envelope. As a step toward harnessing the potential benefits of using active control for flutter suppression, an active flexible wing (AFW) wind-tunnel experimental program has been initiated jointly by NASA and Rockwell International Corporation [1].

Many alternative control concepts are being studied in this program to develop flutter suppression laws to be tested in the wind-tunnel experimental program. The present report summarizes the concept, design, and evaluation of a novel control scheme which results in a robust, low complexity flutter suppression control law. Extensive simulation studies are included to demonstrate that the control law meets all the design constraints set forth to clear the control law for subsequent wind-tunnel tests.

# BASIC CONTROL PROBLEM

The flexible equations of motion of the AFW wind-tunnel model at a fixed dynamic pressure ($\bar{q}$) and Mach number (M) can be approximated by a finite dimensional, constant coefficient differential equation in state variable form as;

$$\begin{bmatrix} \dot{x} \\ \ddot{x} \end{bmatrix} = \begin{bmatrix} 0 & I_n \\ -M^{-1}K & -M^{-1}D \end{bmatrix} \begin{bmatrix} x \\ \dot{x} \end{bmatrix} + \begin{bmatrix} 0 \\ -M^{-1}B \end{bmatrix} u \; ; \; y = C\ddot{x} \qquad (1)$$

where $x \in \Re^n$; $u \in \Re^m$; $y \in \Re^r$ and x is a set of generalized co-ordinates associated with the flexible modes. M, K and D are the generalized mass, stiffness and damping matrices.

B and C are the control and output distribution matrices respectively. u is the control vector and y is the acceleration output vector at physical locations of the wing.

In order to understand the principal characteristics of the flutter phenomenon in a control theoretic setting, the unsteady aerodynamic effects and actuator dynamics are not initially included in the design model. Further only a single-input/single-output control problem is examined. Throughout the text and figures the following short hand notation is used to represent second order transfer functions,

$$s^2 + 2\zeta\omega_n s + \omega_n^2 = (\zeta, \omega) \tag{2}$$

A scalar transfer function representation of Eq. (1) can be written as,

$$\frac{y(s)}{u(s)} = \frac{k_0 s^2}{(\zeta_b, \omega_b)} \prod_{i=1}^{n-1} \frac{(\zeta_{z_i}, \omega_{z_i})}{(\zeta_{p_i}, \omega_{p_i})} \tag{3}$$

where $\Pi$ indicates continued product and the two zeros at the origin are associated with the output being acceleration. The lightly damped zero/pole pairs $(\zeta_{z_i}, \omega_{z_i})$ and $(\zeta_{p_i}, \omega_{p_i})$ are typically in close proximity forming the so called 'Dipole' structure. This structure allows us to initially ignore the high frequency modes and examine a dominant two mode approximation to Eq. (3) of the form;

$$\frac{\ddot{z}_{TIP}(s)}{\delta_{TEO}(s)} = \frac{k_0 s^2}{(\zeta_b, \omega_b)} \frac{(\zeta_c, \omega_c)}{(\zeta_t, \omega_t)} \tag{4}$$

where $\ddot{z}_{TIP}$ is the wing tip acceleration and $\delta_{TEO}$ is the trailing edge outboard control surface deflection (figure 1). The flutter dynamics can be adequately represented by the strong interaction of a bending mode $p_b$ $(\zeta_b, \omega_b)$ and a torsion mode $p_t$ $(\zeta_t, \omega_t)$. Associated with these modes is a critical zero $z_c$ $(\zeta_c, \omega_c)$ whose relative location in the complex plane with respect to the dominant modes plays a key role in the feedback stabilization of the unstable flutter mode. Figure 2 gives a locus of the poles/zeros of

Eq. (4) as a function of the dynamic pressure, $\bar{q}$, for the AFW symmetric flutter model. At low dynamic pressures the torsion mode $p_t$ forms a dipole with the critical zero $z_c$. As the dynamic pressure is increased the dipole bond is broken and the torsion mode becomes more controllable and observable. Indeed the dynamic pressure root locus is typical of all input/output pairs of the active flexible wing (AFW) model.

Now consider a simple feedback gain stabilization scheme as shown in figure 3a for a high dynamic pressure condition (open-loop unstable). As the loop gain $\rho$ is increased, the gain root locus can take either of the forms shown in figures 3b and 3c. In the AFW case the locus takes the form of figure 3c. With increased feedback gain the flutter mode $p_b$ is attracted towards the critical zero $z_c$. The incremental gain required to improve the flutter mode damping progressively increases as $p_b$ approaches $z_c$. In the limit as $\rho \rightarrow \infty$, $p_b$ and $z_c$ ultimately form a dipole. Thus the location of $z_c$ strongly influences the gain required to stabilize the flutter mode and also the achievable improvement in the flutter mode damping.

The allowable gain for feedback stabilization is restricted due to i) actuator rate saturation caused by control motion due to wind-tunnel turbulence, and ii) the possibility of driving some high frequency modes unstable while stabilizing the flutter mode. Thus the design of the control law focuses on the selection of a sub-optimal dynamic compensation scheme to stabilize the flutter mode while meeting the above stated gain constraints. The controller also should possess adequate gain/phase margins to account for parameter uncertainties invariably associated with aeroelastic modeling.

## AFW SYMMETRIC FLUTTER CONTROL PROBLEM

### Design Objectives and Constraints

The primary objective of the design is to increase the flutter onset dynamic pressure boundary. The uncontrolled symmetric flutter for the AFW model in a Freon test medium at M = 0.9 is predicted to occur at $\bar{q}$ = 245 psf. Figure 4 illustrates the violent nature of the

flutter divergence of the AFW wind-tunnel model. For comparison, the mild divergence of the B-52 aircraft is also included for which an active flutter suppression law was successfully flight tested [2]. This comparison highlights the severity of the AFW flutter control problem. In addition, as mentioned earlier, the AFW model will be subjected to significant levels of wind-tunnel turbulence. Consequently this sets a major constraint on the allowable feedback gains to stabilize the flutter mode due to RMS control rate saturation problems. Finally modeling ignorance dictates that adequate stability margins be provided.

## System Model

The AFW system can be represented as a linear time-invariant state variable model for a fixed dynamic pressure and Mach number. The finite element model refined by ground vibration tests has eight elastic modes and eight unsteady aerodynamic lag states. For the controller design a single-input/single-output configuration was selected to properly understand the control problem and synthesize the dynamic compensation. Among the set of acceleration sensors available (figure 1), the wing tip sensor was selected since its response peaks near the flutter frequency and has a substantially attenuated response for higher frequency modes. The trailing edge outboard surface was chosen as the control surface since it has the highest control effectiveness and consequently results in low feedback gain solutions. The trailing edge outboard actuator also has the highest natural frequency compared to the other actuators. However, due to engineering constraints the actuator has the lowest control rate capability (225 deg/sec - no load). The composite model has 27 states including a third order actuator model. When evaluating the gust response of the system a two state Dryden turbulence model was added to the composite system model.

# AN ANALYTICAL SOLUTION TO THE FLUTTER CONTROL PROBLEM

Figure 5 shows the pole/zero map of the AFW system at a reference condition of $M = 0.9$, $\bar{q} = 300$ psf with the test medium being Freon. Using this model, a simple gain feedback as suggested in figure 3a was attempted to stabilize the flutter mode. Figure 6 gives the resulting gain root locus. Although the flutter mode has been stabilized, one of the higher frequency modes is driven unstable. One pair of real roots coalesces and form a conjugate pair with high natural frequency. It is apparent from the root locus that a high gain solution has resulted. The primary cause for this situation is the adverse location of the critical zero $z_c$ near the $j\omega$ axis ($-3.6 \pm j\,70$). Since $z_c$ depends on the sensor/actuator locations, alternative sensor positions were evaluated to get more favorable zero locations (figure 1). The trailing edge outboard actuator was retained due to its superior control power. No substantial improvement in the damping of the critical zero resulted. Thus, the static high gain design reveals that some form of frequency weighted feedback gain (dynamic) compensation is required.

The simplest dynamic compensation is a lead/lag filter of the form $(s+\alpha)/(s+\beta)$. This compensator structure was explored in [3] using a multi-input/multi-output formulation. The study yielded stable designs with low feedback gains in the flutter frequency range (50-80 rad/sec), resulting in acceptable RMS control deflections and rates subject to wind-tunnel turbulence. However, the gains at the low frequency spectrum (0.5-2 rad/sec) were substantially higher due to the large separation between the zero ($\alpha$) and the pole ($\beta$) of the lead/lag filter that was needed for the solution. This control law is prone to control saturation problems resulting from the closed-loop system being excited by error signals generated through quantization effects of low resolution analog-to-digital converters. A similar single-input/single-output solution with second order compensation proposed in [4] is also prone to this saturation problem. The primary motivation to seek these filter

solutions was to make sure that the filter poles were well damped so that closed-loop instability due to filter root divergence is avoided.

In light of the above experience, the problem of finding a minimal gain solution was reexamined using the analytical framework of Eq. (4) and the generic root locus of figure 3c. As observed before, the migration of the unstable flutter mode into the left half complex plane is inhibited by the presence of the critical zero. In order to alleviate this problem the compensator was allowed to have low damped poles with a structure of the form;

$$H(s) = \frac{(\zeta_{z_f}, \omega_{z_f})}{(\zeta_{p_f}, \omega_{p_f})} \tag{5}$$

Figure 7 is a schematic of the new compensation scheme. An anti-aliasing filter is used since the compensator is mechanized on a digital computer. A washout filter is included to eliminate acceleration sensor bias errors and does not substantially contribute to the compensation. The filter structure of Eq. (5) suggests one obvious solution, namely to have the filter pole cancel the effect of the critical zero (pole/zero cancellation!) and have the zero of the filter moved farther into the left half plane. Figure 8 is the resulting root locus ($M = 0.9$, $\bar{q} = 300$ psf) with the filter pole $p_f$ at $-3.6 \pm j\ 70$ and $z_f$ at $-70 \pm j\ 70$. It is apparent that the flutter mode has been stabilized without disturbing the other modes. Thus a minimal control effort solution has been derived. Since the filter pole $p_f$ forms a dipole with the critical zero $z_c$ the compensator filter H(s) is called a 'Dipole' filter.

The analysis in this section has thus: i) identified the fundamental constraint for feedback stabilization of the flutter mode in terms of the adverse location of a system zero designated as a critical zero $z_c$, ii) recognized the need to allow the selection of low damped roots for the compensation filters in the proximity of the critical zero to effectively alleviate

the zero's unfavorable location in the complex plane and iii) provided a simple analytical solution in the form of a 'Dipole' filter to stabilize the flutter mode with minimal gain.

## PRACTICAL IMPLEMENTATION ISSUES

The dipole filter solution presented in the previous section obviously raises questions such as: i) how valid is the existence of the critical zero, ii) how accurately can it be determined, and iii) how sensitive is the proposed dipole filter solution is to variations in the location of the critical zero. Since the modeling structure of the aeroelastic system in the form of Eq. (1) originates from the classical vibration dynamics of a multi-degree-of-freedom spring-mass-damper system, it is reasonable to conclude the existence of a transfer function zero in the vicinity of the dominant bending and torsion modes as depicted in figure 2.

Accurate experimental determination of the damping of the critical zero by parameter estimation techniques may be difficult since the zero almost forms a dipole with the torsion mode at subcritical dynamic pressures (below flutter onset dynamic pressure) where the plant identification experiments are conducted. As a first approximation $z_c$ can be taken as the torsion mode $p_t$ itself at the highest subcritical $\bar{q}$. Thus the sensitivity of the proposed compensation scheme to uncertainty in the location of the critical zero is important. Towards this end the damping of the compensation filter root $p_f$ was progressively increased and the gain root locus generated. Figures 9 and 10 depict the root loci for filter poles at $-7 \pm j\,70$ and $-10 \pm j\,70$, respectively, for a reference condition of $M = 0.9$, $\bar{q} = 300$ psf. The filter zero remained fixed at $-70 \pm j\,70$.

Comparison of the root loci in figures 8 through 10 reveals that no substantial change in root locus branch patterns has resulted. However, as the filter pole damping is increased the static gain (k) required to stabilize the flutter mode increases. Also, as the filter root damping is increased the sting mode (mode with the lowest natural frequency) is predicted

to become unstable at large gains. The pole/zero cancellation design has excellent gain margin but very poor phase margin. The increase of the filter pole damping has the effect of trading gain margin with phase margin. Of course, excessive increase in the filter pole damping renders the compensation scheme ineffective. A filter pole location at $p_f = -7 \pm j70$ was found to be the best compromise solution from both gain and phase margin considerations. This sensitivity study also substantiates that the proposed analytical solution is not overly sensitive to accurate knowledge of the damping of the critical zero. Nonlinear simulation studies, to be discussed subsequently, also corroborated this observation which was based on linear analysis.

## CRITERIA FOR VALIDATING CONTROL LAWS

The following criteria are set up to evaluate the performance of the control laws with a view toward certifying them for subsequent evaluation in the wind-tunnel test program.

i) Gain margin of ± 6dB and phase margin of ± 45 deg.
ii) No RMS control rate saturation should occur for 1 foot/sec RMS input.
iii) Stability robustness throughout the operating dynamic pressure range (50–350 psf).
iv) Stability robustness to modeling uncertainty introduced by varying the vibration mode frequencies and damping.

The primary tools for evaluating the control laws are: i) a nonlinear batch simulation of the AFW system designated as the 'ACSL' simulation [1] and ii) a time synchronized scaled-real-time simulation with the digital control computer in-the-loop and designated the 'Hot Bench' simulation [1].

Among the criteria listed above, the RMS rate saturation constraint can be used to estimate the upper bound on the feedback gains. Assume the gust response is dominant at the flutter frequency. Then the control deflection, assuming simple harmonic motion, is given by;

$$\delta_{TEO} = k \ddot{z}_{TIP} \sin \omega t \tag{6}$$

where $\omega$ is the flutter frequency (approx 70 rad/sec). Then the control rate is

$$\dot{\delta}_{TEO} = k \omega \ddot{z}_{TIP} \cos \omega t \tag{7}$$

The peak no load rate capability of the TEO surface is 225 deg/sec. This translates to an RMS rate of 75 deg/sec assuming random excitation. From Eq. (7), for $\omega$ = 70 rad/sec and max RMS $\dot{\delta}_{TEO}$ = 75 deg/sec, the max RMS $\delta_{TEO}$ = 1.1 deg and maximum control gain k = 1.1 deg/g at the flutter frequency. Notice in this analysis that the reduction of control rate capability due to aerodynamic load (hinge moment) has been neglected. This effect is, however, explicitly included in the ACSL simulation.

## LINEAR SIMULATION RESULTS

A single-input/single-output output design, designated Control Law 1, using the trailing edge outboard control surface and wing tip acceleration sensor was analyzed. The dipole filter pole $p_f$ is located at $-7 \pm j\ 70$ and the zero $z_f$ is located at $-70 \pm j\ 70$. The nominal feedback gain to stabilize the flutter mode is k = 0.11 deg/g. The washout filter is the same as in figure 7. The frequency response of the washout filter and the dipole filter in cascade is shown in figure 11. The corresponding time response of the control motion $\delta_{TEO}$ to a 1 g step wing tip acceleration input is given in figure 12. The controller is evaluated over a range of dynamic pressures (100–400 psf) at M = 0.9 in Freon using linear models at discrete dynamic pressure conditions. The fixed gain controller exhibited stability robustness with respect to the dynamic pressure variations. Figure 13 depicts the damping of the dominant modes for a range of dynamic pressures. Notice that the structural damping ($g = 2\zeta$) of the closed-loop roots is in excess of the minimum requirement throughout the dynamic pressure range.

Using a variational model approach in the linear simulation setup, the stability robustness of the controller to modeling uncertainties was also analyzed. The basis for derivation of the variational model (VAR) was an analytical ten flexible mode finite element model (FEM) refined to match the eight dominant modes observed during ground vibration tests. The VAR model differed from the final reference models (GVT) used in the Linear, ACSL and Hot Bench simulations in the method used to correct the modal characteristics to match ground vibration test data. Without going into the details of the model derivation, it was considered sufficient to use the VAR model as a perturbation model for sensitivity analysis. Figure 14 shows the differences in frequency response of the FEM, GVT and VAR models (M = 0.9, $\bar{q}$ = 300 psf). The controller performed satisfactorily when the VAR model is substituted for the GVT model. As a result, the controller is robust to a simultaneous gain variation of approximately 5 dB and phase lag of 15 deg near the flutter frequency. However substitution of the FEM model makes the closed-loop system unstable. This is to be expected because of the large phase deviations, nearly 80 degrees, in the flutter frequency range between the GVT and FEM models. Thus the feedback system is deemed robust to moderate modeling uncertainties.

## ACSL SIMULATION RESULTS

### Control Law 1

The analog form of Control Law 1 was converted to digital form using the Tustin transformation with a sampling interval of 5 milliseconds. The digital form of the controller was used in the ACSL and Hot Bench simulations.

Gain margin.

The gain margins were determined in the ACSL simulation by varying a scalar loop gain parameter from the nominal value set by k (similar to the root locus gain parameter $\rho$ in figure 7). The gain is increased/decreased until the closed-loop system becomes unstable. The onset of instability is determined when the system response diverges to a

doublet input applied to the control channel. Figure 15 shows a typical ACSL simulation time response history. Figure 16a summarizes the gain margin boundaries for Control Law 1. The nominal gain for these results is k = 0.33 deg/g. The controller meets the gain margin requirements up to a dynamic pressure of 350 psf. An advantage of the controller is the infinite gain reduction margin in the subcritical dynamic pressure range where the open-loop system is stable.

Phase margin.

In the ACSL simulation there is no convenient way to introduce frequency independent phase shift as the phase margin definition demands. However, from a practical perspective phase uncertainty in a system is generally manifested as a frequency dependent phase lag which is typically modeled as a pure time lag and approximated by Padé filters with appropriate cutoff frequencies. For the present study a simpler mechanization of the time lag is adopted. The ACSL simulation has a fourth order Butterworth filter to simulate the anti-aliasing filter. The nominal cutoff frequency, fco, was 100 Hz. By reducing the cutoff frequency, fco, it was possible to generate phase lag in the flutter frequency range without introducing gain attenuation. Figure 17 shows the gain and phase characteristics of the Butterworth filter as a function of fco in Hz. By varying fco, phase lag was introduced into the system until the system becomes unstable as determined by response trajectories. The loop gain was held constant at k = 0.33 deg/g. The phase reduction margin was computed and the frequency of divergence was also noted. The divergence frequency indicates which branch of the root locus is driven to the right half complex plane. Figure 16b summarizes the ACSL phase reduction margin results. The phase margin requirements are met up to a dynamic pressure of approximately 325 psf.

RMS acceleration / control response to wind-tunnel turbulence.

The ACSL simulation includes an appropriately scaled Dryden turbulence model to generate random wind-tunnel turbulence. This feature was used to generate RMS response

over a range of dynamic pressures for both open-loop (subcritical $\bar{q}$) and closed-loop system with a nominal gain k = 0.33 deg/g. Figure 18 summarizes the RMS response for a 1 ft/sec RMS gust input. The feedback system has lower RMS accelerations at the wing tip compared to the uncontrolled system in the subcritical dynamic pressure range. The RMS control rate and displacement are approaching the limits at a dynamic pressure of 350 psf.

Robustness of controller.

In the ACSL simulation the robustness of Control Law 1 to model ignorance was evaluated by computing the gain and phase margins when the plant was changed from the reference design condition M = 0.9 (Freon) symmetric. These off-design plant reference conditions are: i) Freon, M = 0.9, antisymmetric model, ii) Freon, M=0.8, symmetric and antisymmetric models, and iii) M = 0.5, symmetric and antisymmetric models with air as test medium. The controller performed satisfactorily up to 350 psf with all Freon models and up to 325 psf with the air models.

From the results of the nonlinear simulation studies it can be concluded that Control Law 1 will perform satisfactorily up to a dynamic pressure of 350 psf with Freon as the test medium. This indicates that the controller increases the operating flutter dynamic pressure envelope by 40 percent, while meeting all the criteria set forth to certify the control law for wind-tunnel test.

## Control Law 2

With a view toward reducing the control activity on the trailing edge outboard surface due to wind-tunnel turbulence, a second control law was considered. The effect of including a second control surface to share the work load was investigated. The candidate control surfaces were the leading edge outboard and trailing edge inboard surfaces. The trailing edge inboard surface is preferred since it is favorably loaded aerodynamically. Figure 19 shows the schematic of Control Law 2. The dipole and washout filters are the

same as used in Control Law 1 and the control gain ratio $|k_2/k_1|$ was optimized using root locus analysis. Figure 20 shows the gain root locus for a gain ratio $|k_2/k_1| = 0.5$. The feedback polarity for the control surfaces was chosen such that the rates on the outboard surfaces were reduced. (In this case the character of the structural modes required that the control surfaces have opposite signs.) Table 1 summarizes the achievable reduction in RMS control activity of the trailing edge outboard surface for two different gain ratios, $|k_2/k_1|$. ACSL simulations revealed no substantial reduction in gain and phase margins for a gain ratio of 0.5. For a gain ratio of 1, at higher dynamic pressures (greater than 325 psf) gain margin requirements are not met. Thus Control Law 2 was certified for experimental use using $|k_2/k_1| = 0.5$.

## HOT BENCH SIMULATION RESULTS

After satisfactory completion of the nonlinear simulations Control Law 1 was evaluated in the Hot Bench simulation. The controller channel was excited by a doublet pulse and the system response was recorded as the dynamic pressure was progressively increased. The controller stabilized the system up to $\bar{q}$ = 350 psf. This result is consistent with the ACSL simulation results. The system became unstable at about 360 psf. The AFW digital control computer adds an additional phase shift into the loop due to the sampling effects (sampling rate = 200 samples/sec in real time). Figure 21 shows the frequency response of the control computer indicating the classical delay transfer function. The computer adds a phase lag of 18 deg at 10 Hz. Sinusoidal frequency sweep excitations were applied to the control channel for both the open- and closed-loop systems at a subcritical dynamic pressure of 200 psf. Figure 22 compares the wing tip acceleration response. The attenuation of the peak response due to feedback is apparent. Figure 23 is a comparison of the transfer functions derived from sine sweep experiments. The frequency signature of the closed-loop transfer function is substantially different. There are two peak responses at 7.6 Hz and 13.8 Hz as compared to the single peak at 10 Hz for the open-loop

case. Indeed this change in frequency signature can be effectively used in wind-tunnel tests at subcritical $\bar{q}$ to confirm satisfactory (predicted) performance of the controller. This frequency signature can also be inferred from gain root locus plots. The transfer functions were also derived using linear models to correlate the Hot Bench results. Figure 24 shows the transfer functions for the same reference condition of $\bar{q}$ = 200 psf. To generate these plots a first order Padé approximation at a cutoff frequency of 100 Hz was added to the model to account for the AFW control computer phase delay. The match between the linear analysis and Hot Bench is excellent.

## CONCLUSIONS

The control of the symmetric flutter divergence of the AFW wind-tunnel model has been studied. The following conclusions can be drawn;

i) The presence of a critical system zero close to the jω axis sets a limit on the minimum static feedback gain required to stabilize the flutter mode. The critical zero also sets a limit on the achievable improvement in the flutter mode damping.

ii) Static gain solutions are not practical since they tend to drive high frequency modes unstable and violate the RMS control rate constraints in the presence of wind-tunnel turbulence. This leads to the selection of a dynamic compensation scheme to stabilize the flutter mode.

iii) In order to effectively compensate for the adverse location of the system zero and to achieve minimal control effort solutions, poles of the compensator filters should be chosen with low damping close to the critical zero. Using this hypothesis a compensator filter called a 'Dipole' filter is derived which analytically provides a simple robust compensation scheme for flutter suppression.

iv) Linear, ACSL, and Hot Bench simulation studies indicate that the simple dipole filter compensation scheme effectively increases the operating flutter dynamic pressure boundary by 40 percent, while meeting all the design constraints such as gain/phase margins, RMS control displacement and rate limits, and robustness to dynamic pressure variations and modeling uncertainties.

v) Although the trailing edge outboard control surface alone is capable of achieving a 40 percent increase in flutter dynamic pressure boundary, adding the trailing edge inboard control surface with a control gain ratio of 0.5 reduces the RMS control rate activity of the trailing edge outboard surface.

## REFERENCES


[1] Noll, T.E., et al.: Aeroservoelastic Wind-Tunnel Investigations using the Active Flexible Wing Model- Status and Recent Accomplishments, AIAA/ASME/ASCE/AHS 30th Structures, Structural Dynamics and Materials Conference, AIAA paper 89-1168, April 3-5, 1989.

[2] Roger, K.L., and Hodges, G.E.: Active Flutter Suppression - A Flight Demonstration, J. Aircraft, Vol. 12, No. 6, pp 551-556, June 1975.

[3] Srinathkumar, S., and Adams, W.M.: Active Flutter Suppression using Invariant Zeros / Eigensystem Assignment, AIAA Guidance, Navigation and Control Conference, AIAA paper 89-3610, Aug 14-16, 1989.

[4] Schmidt, D.K., and Chen, T.K.: Frequency Domain Synthesis of a Robust Flutter Control Law, J. Guidance and Control, Vol. 9, No. 3, pp 346-351, May-June 1986.


## ACKNOWLEDMENTS


The author acknowledges the support for this research by a NRC-NASA Research Associateship award.

17 INTENTIONALLY BLANK

Table 1 RMS response comparisons - Control Laws 1 and 2.

| Control Law | Gain $k_1$ (deg/g) | Gain Ratio $\lvert k_1 / k_2 \rvert$ | $\bar{q}$ (psf) | $\ddot{z}_{TIP}$ (g's) | $\ddot{z}_{TEO}$ (g's) | $\delta_{TEO}$ (deg) | $\dot{\delta}_{TEO}$ (deg/s) | $\delta_{TEI}$ (deg) | $\dot{\delta}_{TEI}$ (deg/s) |
|---|---|---|---|---|---|---|---|---|---|
| 1 | 0.33 | 0 | 250 | 0.63 | 1.70 | 0.51 | 47.2 | – | – |
| 1 | 0.33 | 0 | 300 | 0.74 | 2.12 | 0.64 | 59.0 | – | – |
| 2 | 0.22 | 0.5 | 250 | 0.67 | 1.68 | 0.42 | 37.8 | 0.2 | 17.2 |
| 2 | 0.22 | 0.5 | 300 | 0.81 | 1.96 | 0.47 | 46.0 | 0.24 | 22.5 |
| 2 | 0.11 | 1.0 | 250 | 0.62 | – | 0.24 | 19.0 | 0.22 | 17.6 |

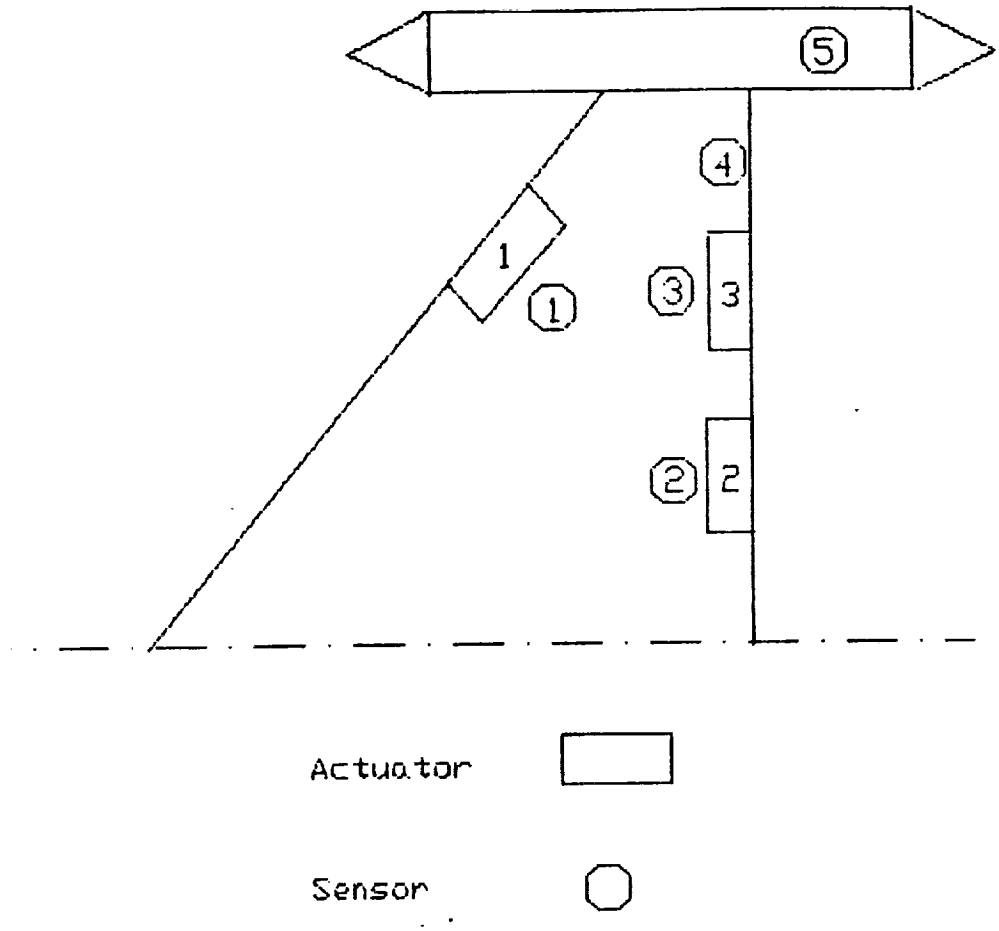


Figure 1 AFW sensor and actuator locations.

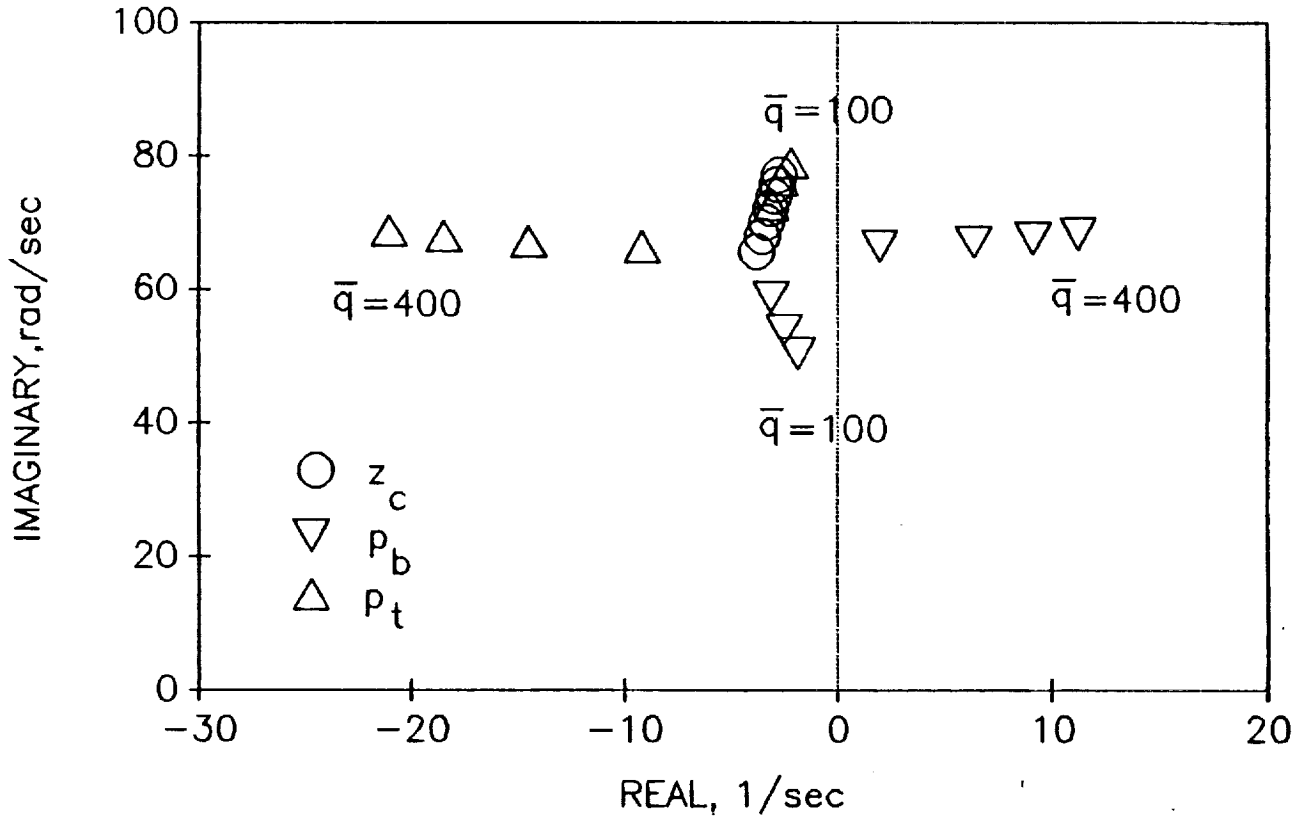


Figure 2 Dynamic pressure root locus of dominant modes.

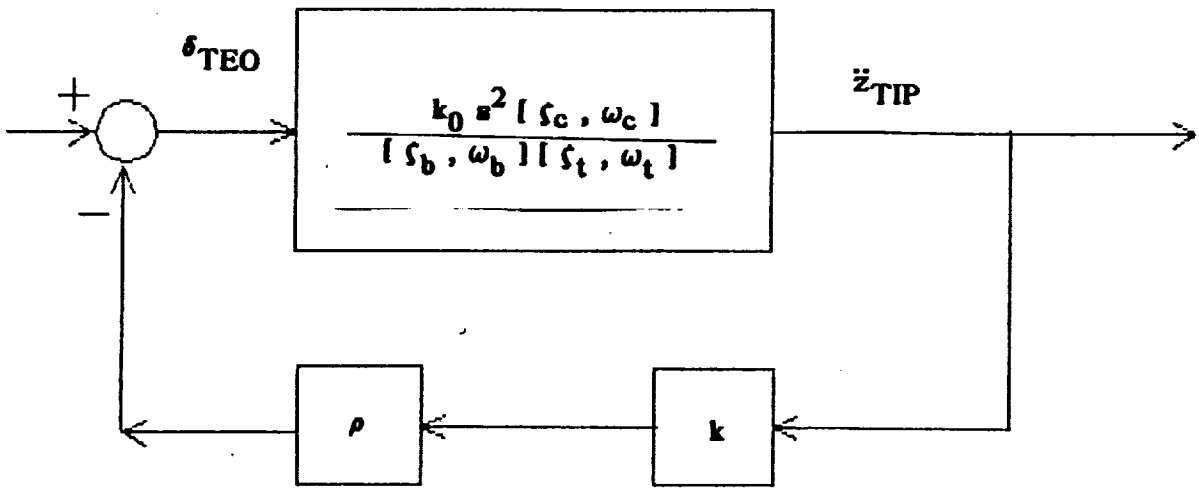


Fig 3a.

**ρ : Root locus gain**

**k : Gain Constant deg/g**

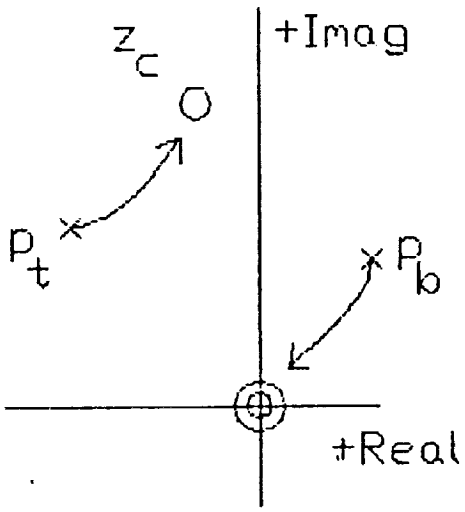


Fig 3b.

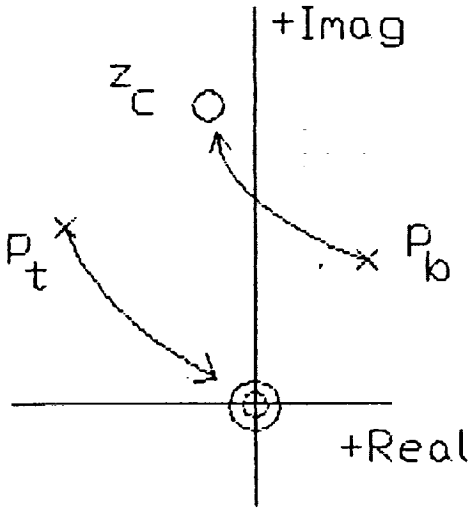


Fig 3c.

Figure 3 Generic root locus for dominant modes.

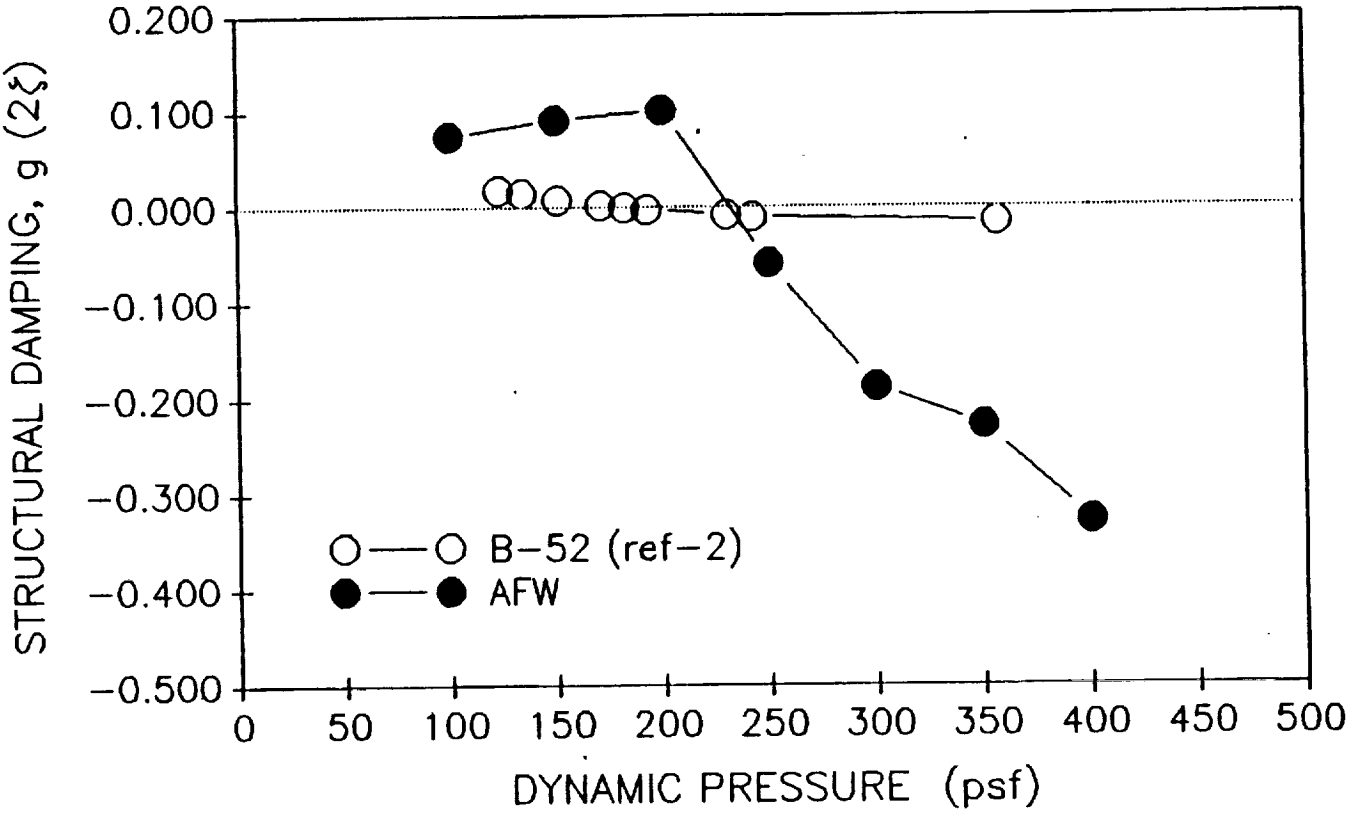


Figure 4 AFW flutter mode damping divergence.

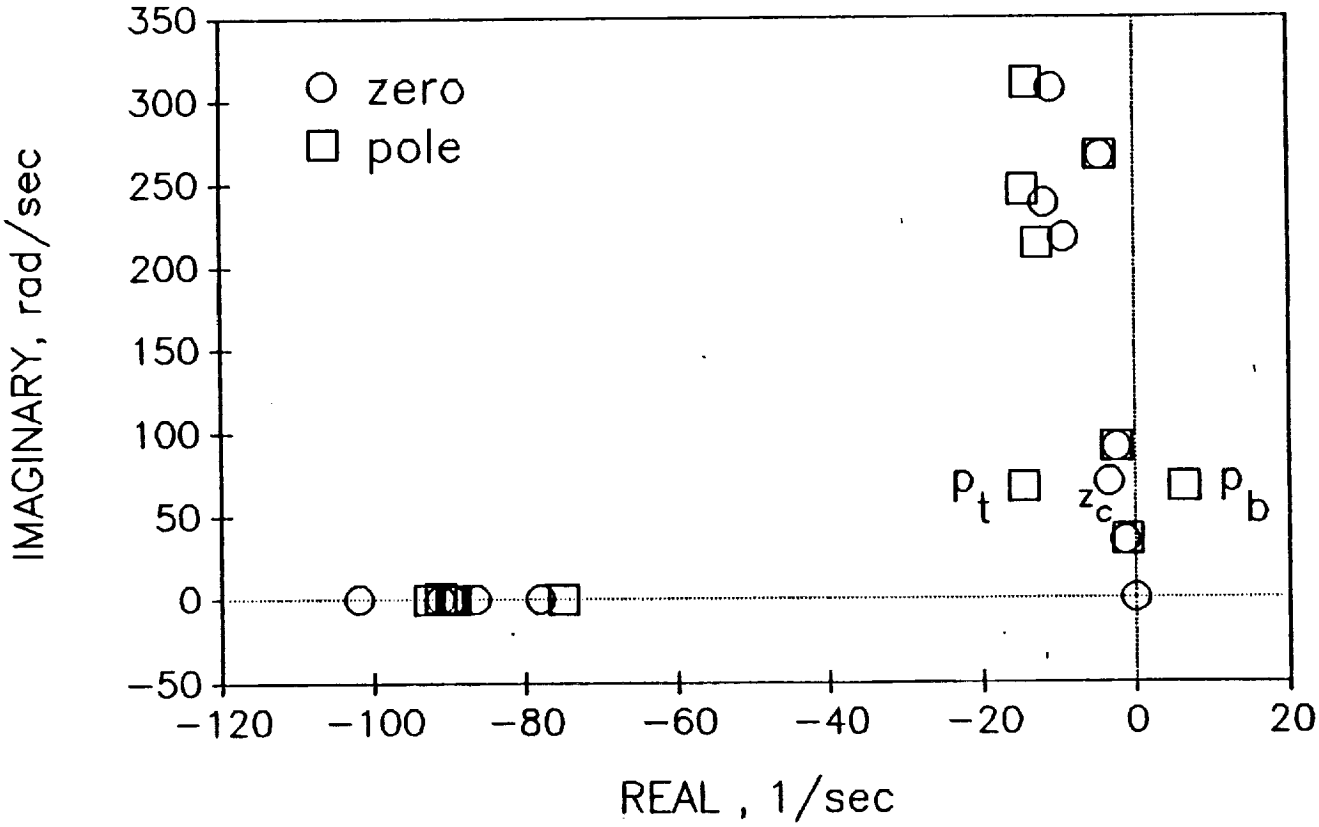


Figure 5 Pole / zero map of AFW symmetric model.

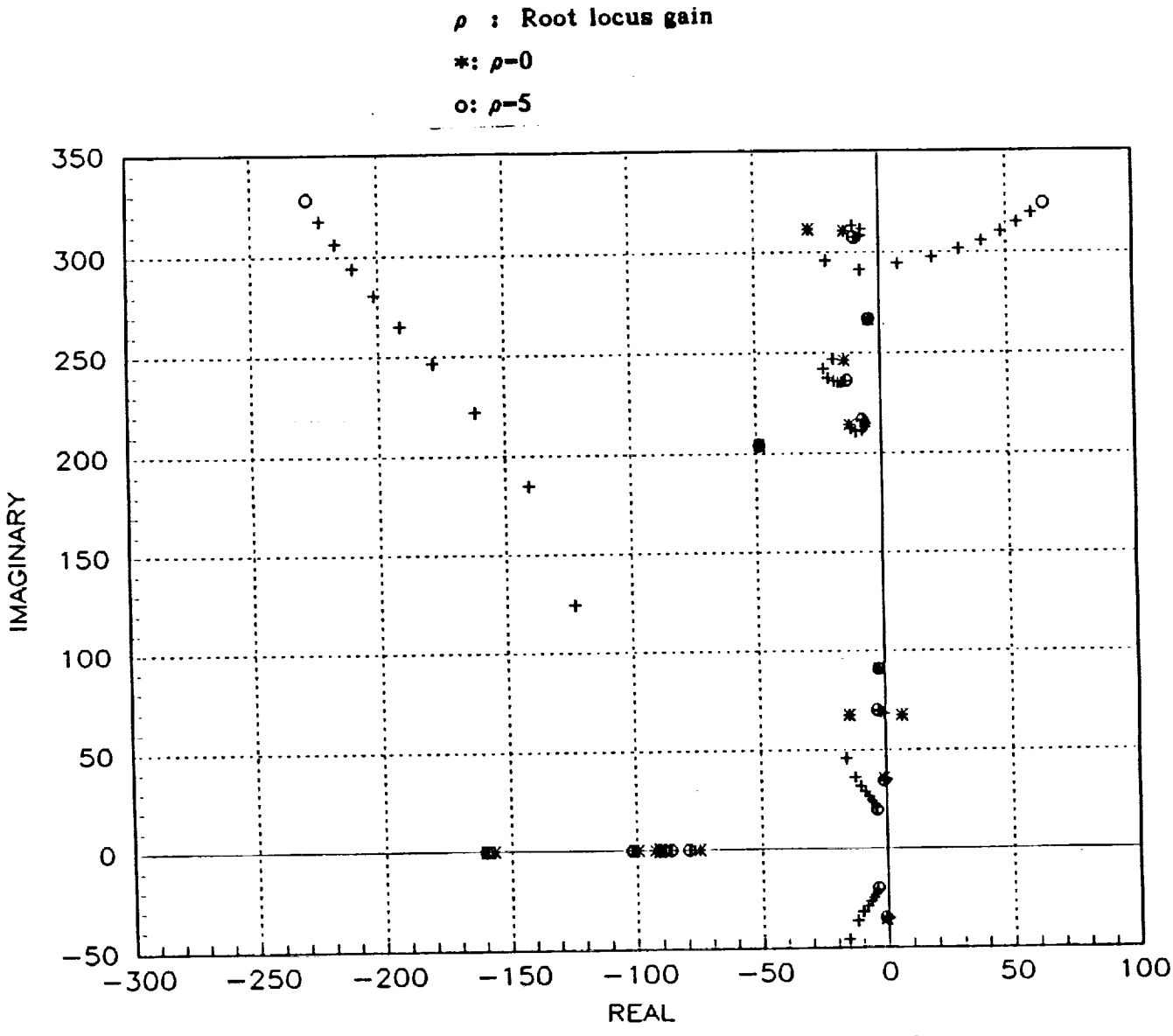


Figure 6 Gain root locus - constant gain feedback (k = 0.22 deg/g)/.

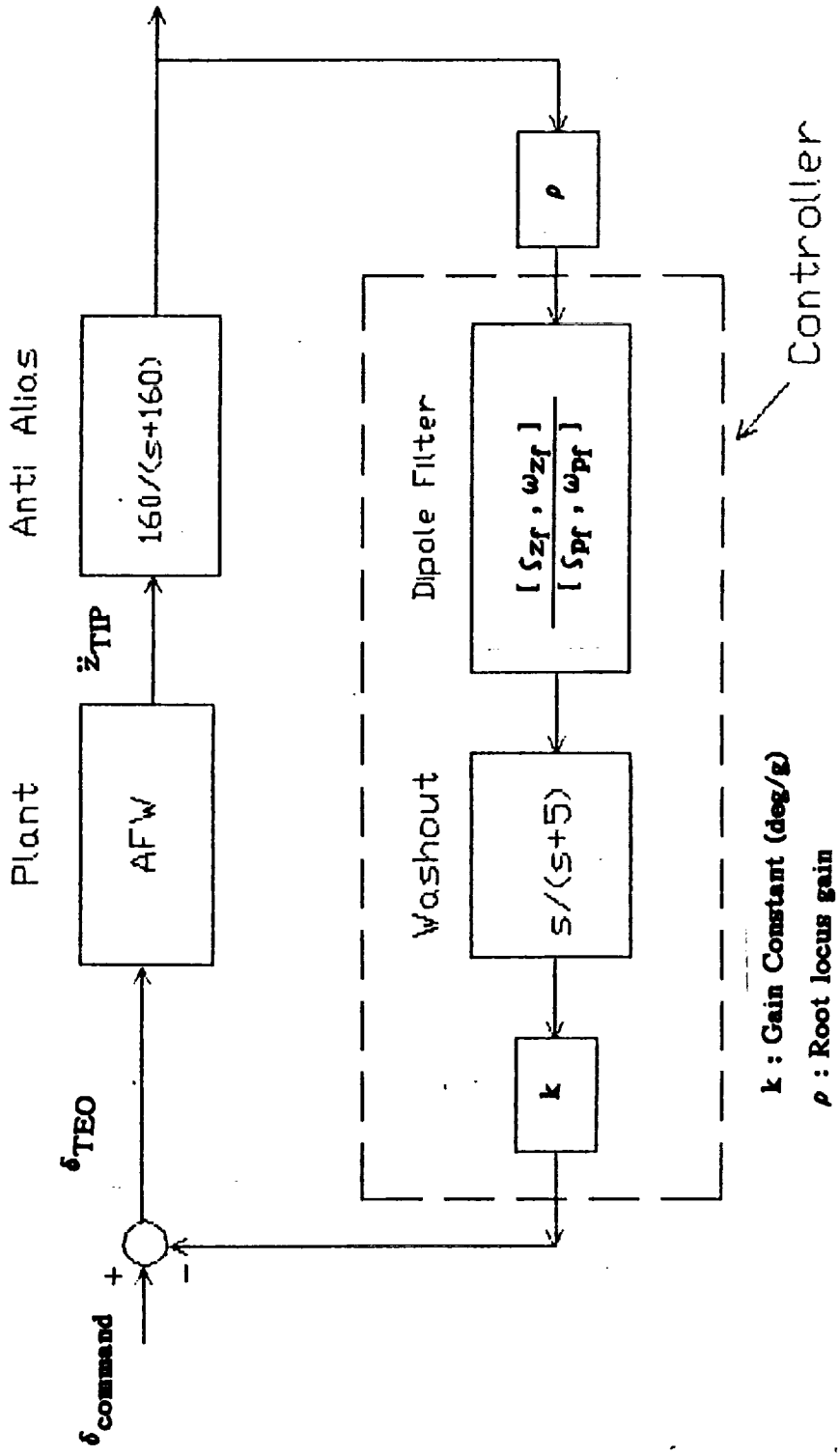


Figure 7 Dipole filter compensation scheme.

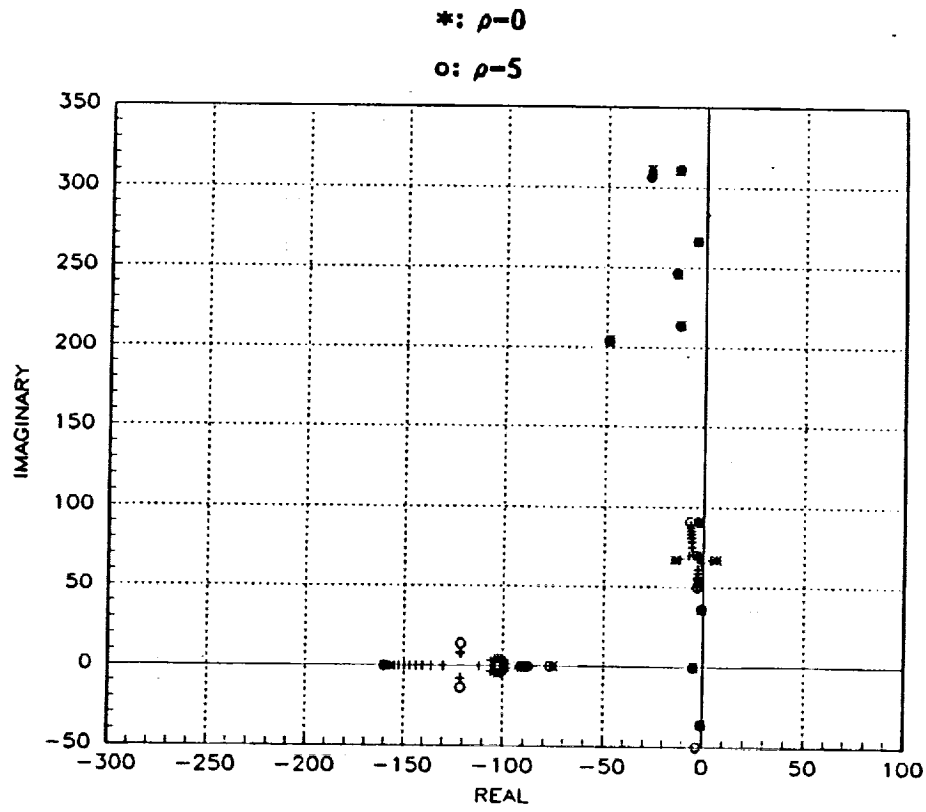


Figure 8a Gain root locus - complete ($p_f = -3.6 \pm j\,70$ ; $k = 0.055$ deg/g).

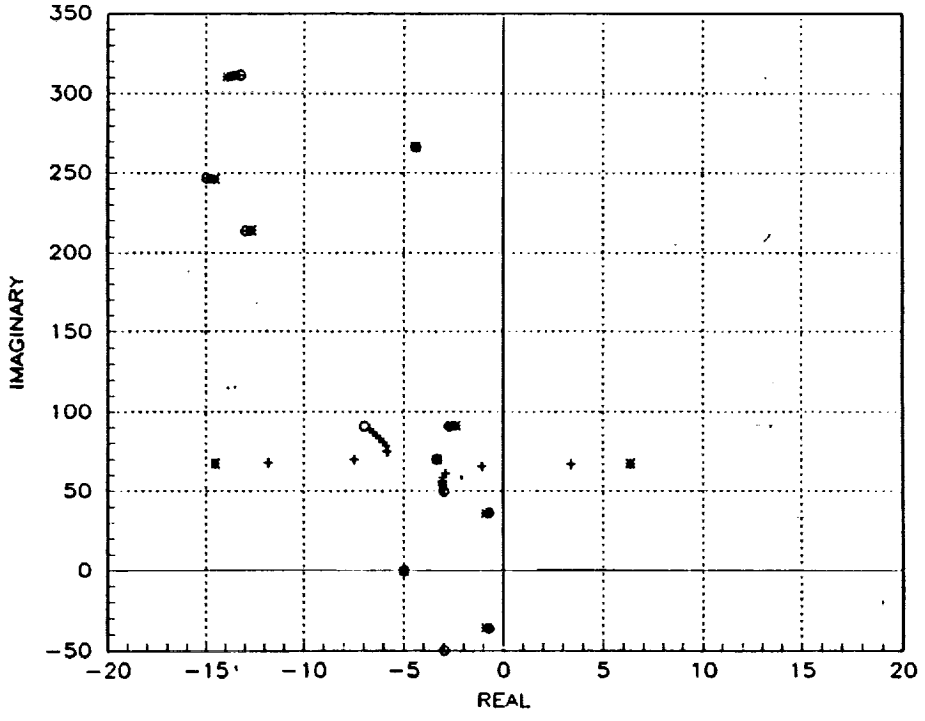


Figure 8b Gain root locus - expanded ($p_f = -3.6 \pm j\,70$ ; $k = 0.055$ deg/g).

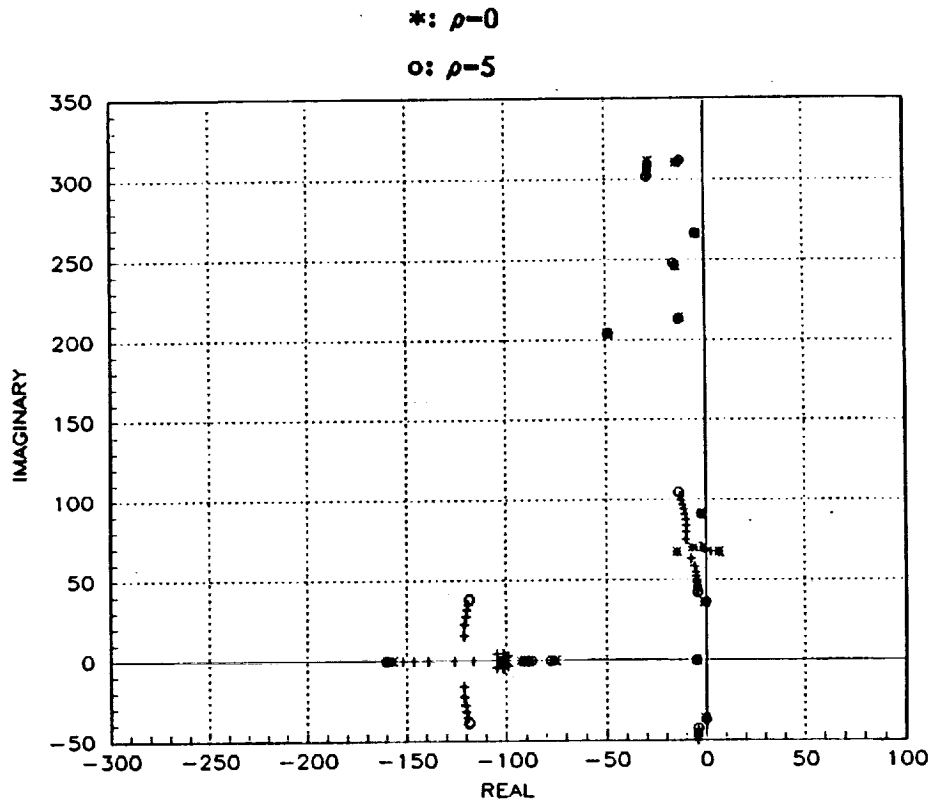


Figure 9a Gain root locus - complete ($p_f = -7.0 \pm j\,70$ ; $k = 0.11$ deg/g).

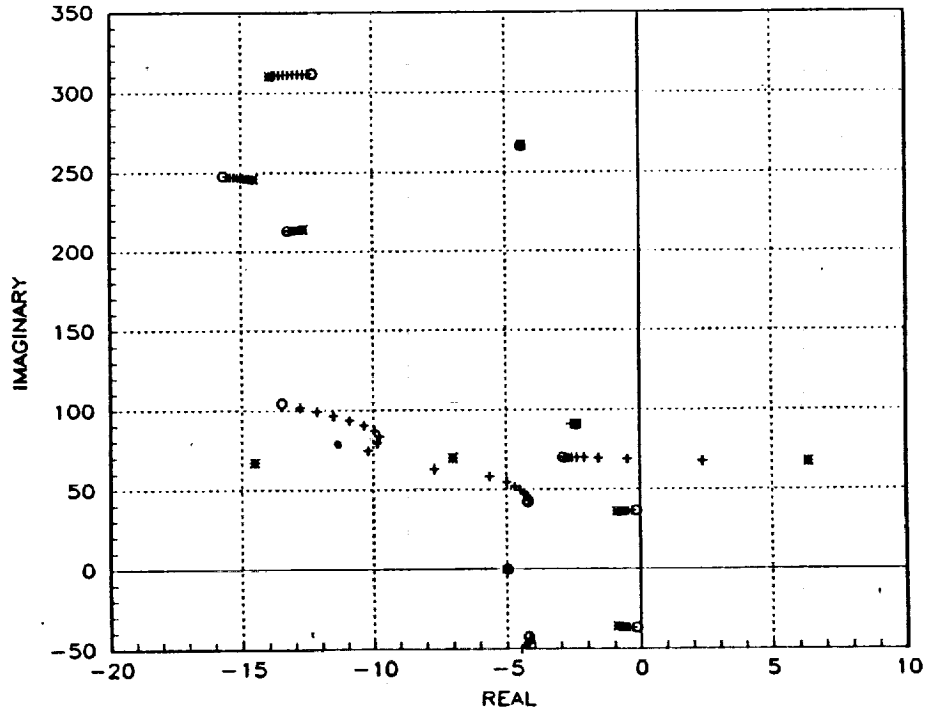


Figure 9b Gain root locus - expanded ($p_f = -7.0 \pm j\,70$ ; $k = 0.11$ deg/g).

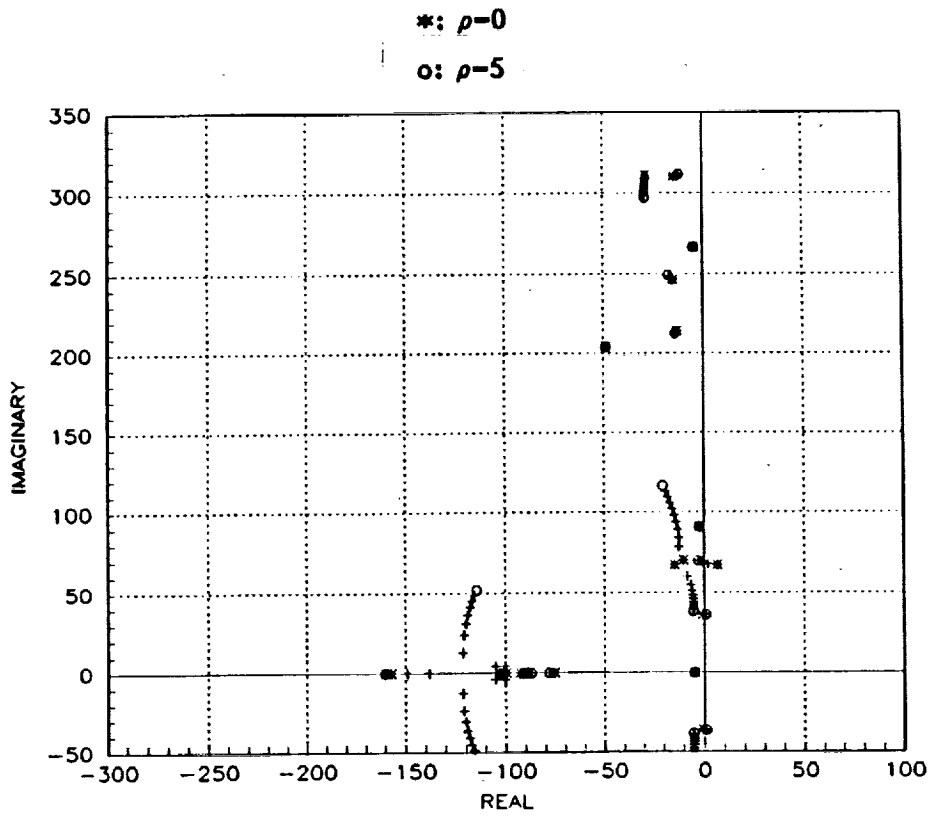


Figure 10a Gain root locus - complete ($p_f = -10.0 \pm j\,70$ ; $k = 0.165$ deg/g).

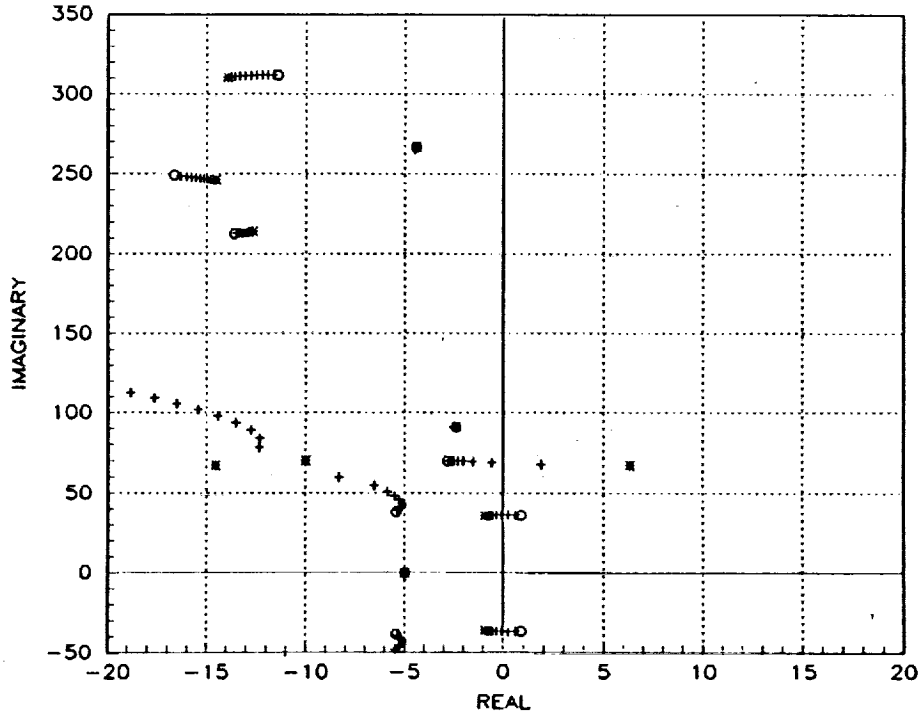


Figure 9b Gain root locus - expanded ($p_f = -10.0 \pm j\,70$ ; $k = 0.165$ deg/g).

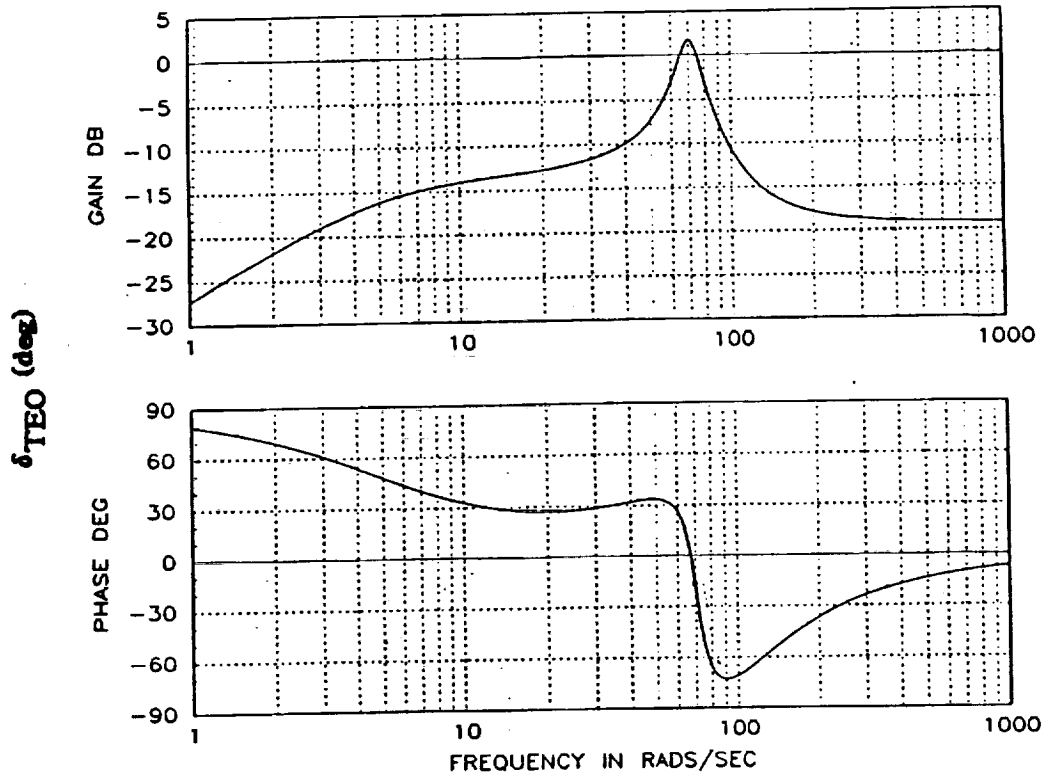


Figure 11 Frequency response of controller ($p_f = -7.0 \pm j\,70$ ; $k = 0.11$ deg/g).

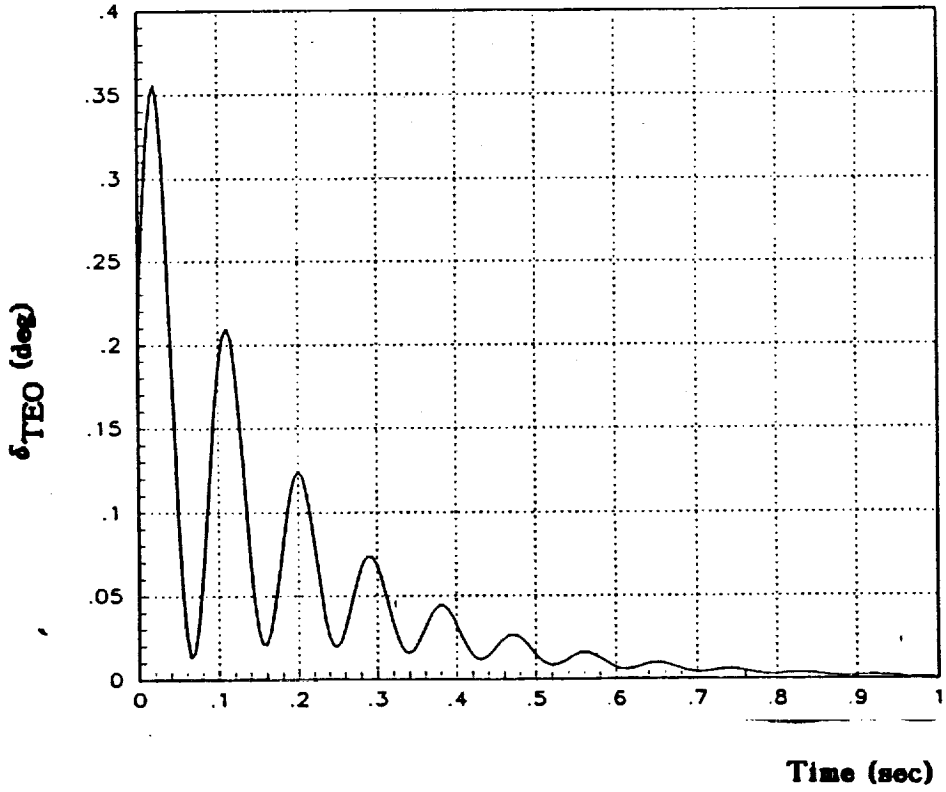


Figure 12 Time response of controller to 1 g step tip acceleration input.

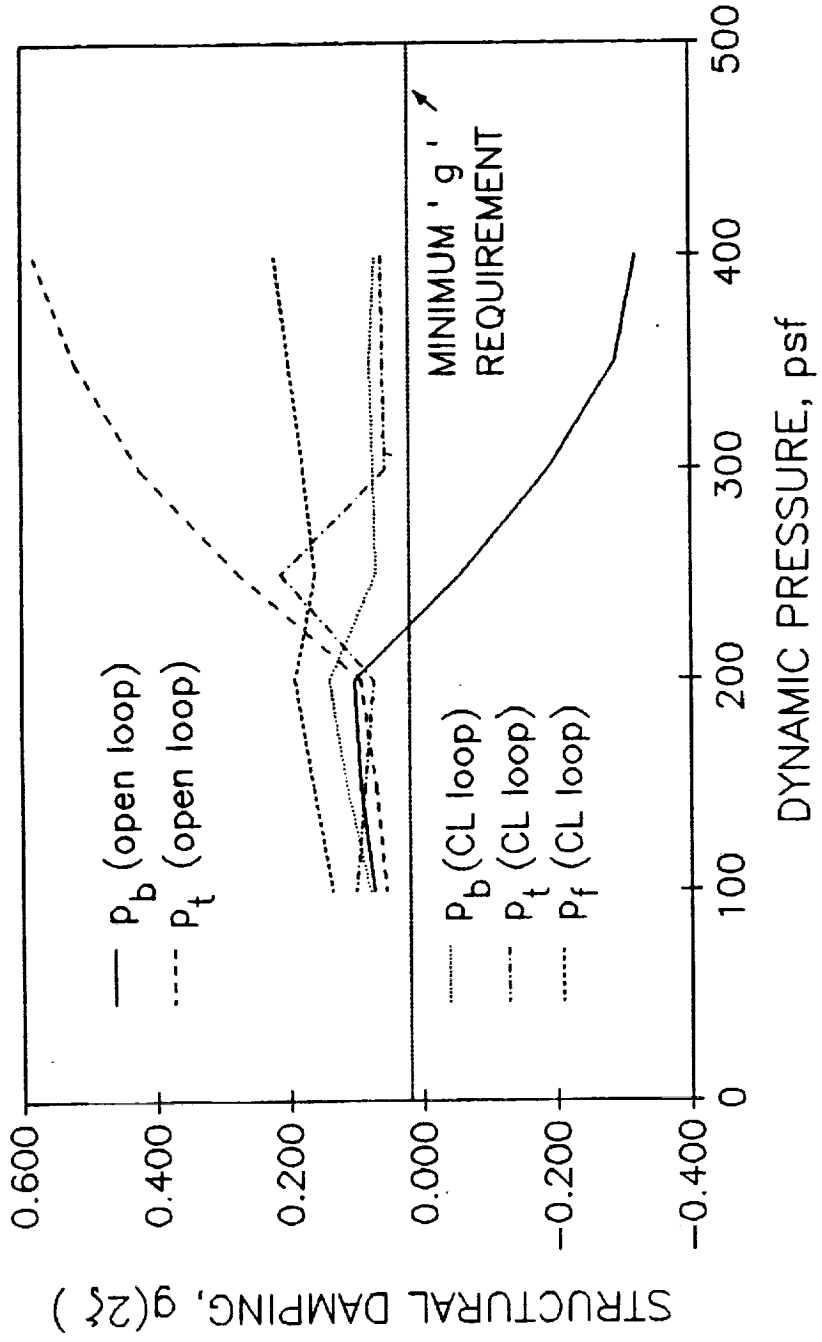


Figure 13 Dominant mode damping as a function of $\bar{q}$.

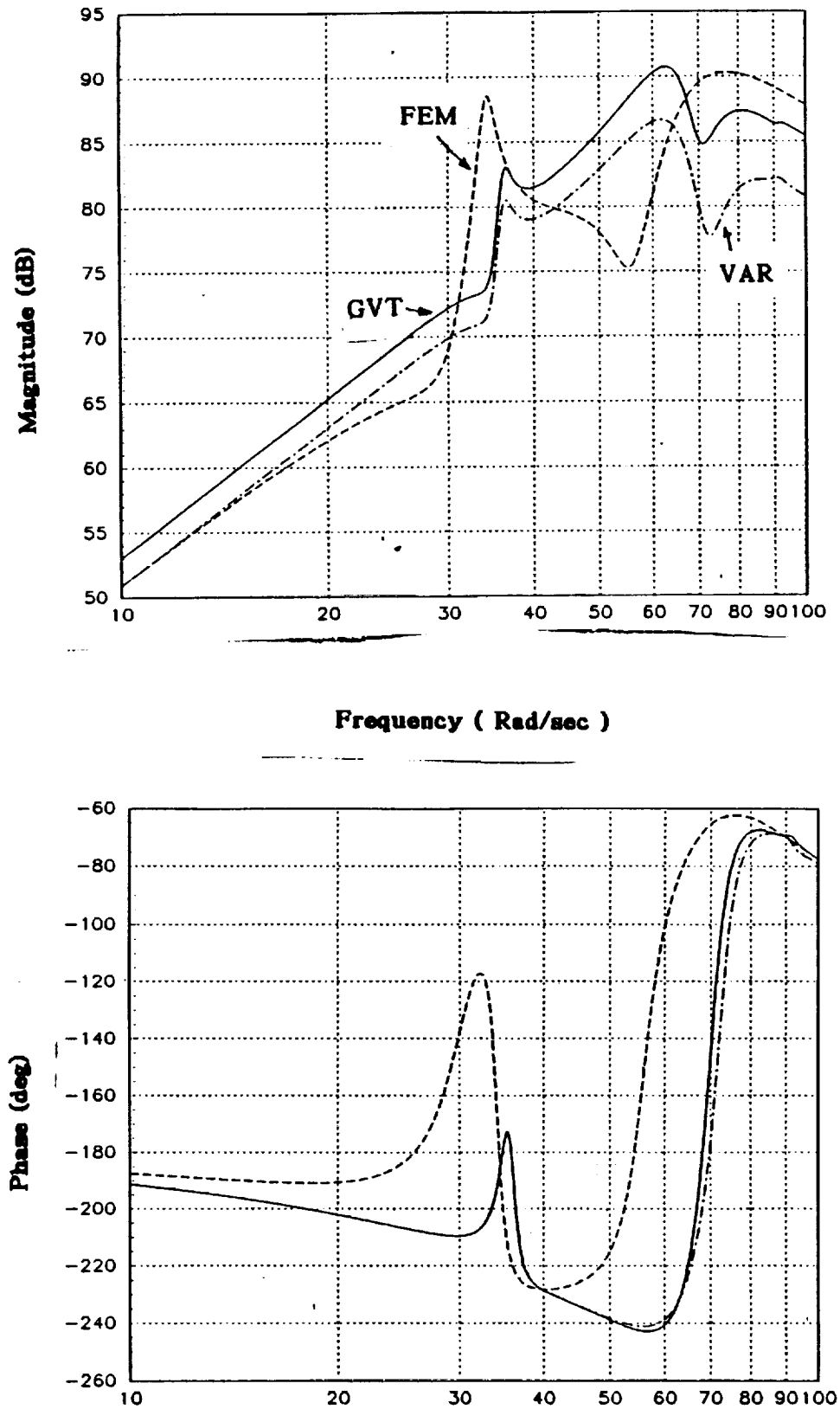


Figure 14 Frequency responses of variational models (FEM, GVT, and VAR).

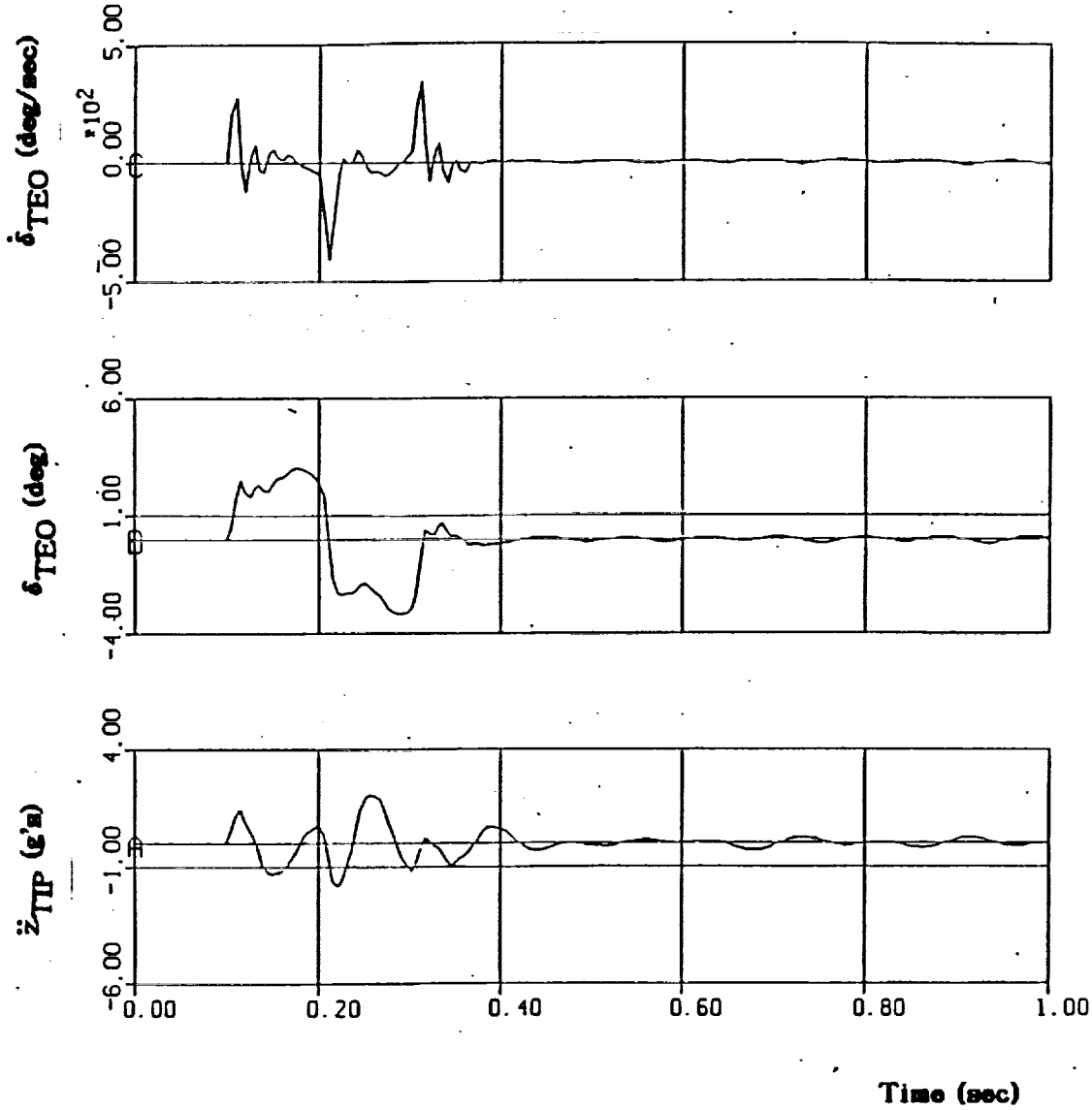


Figure 15 Typical ACSL simulation time response history
(doublet command to trailing edge outboard control surface ).

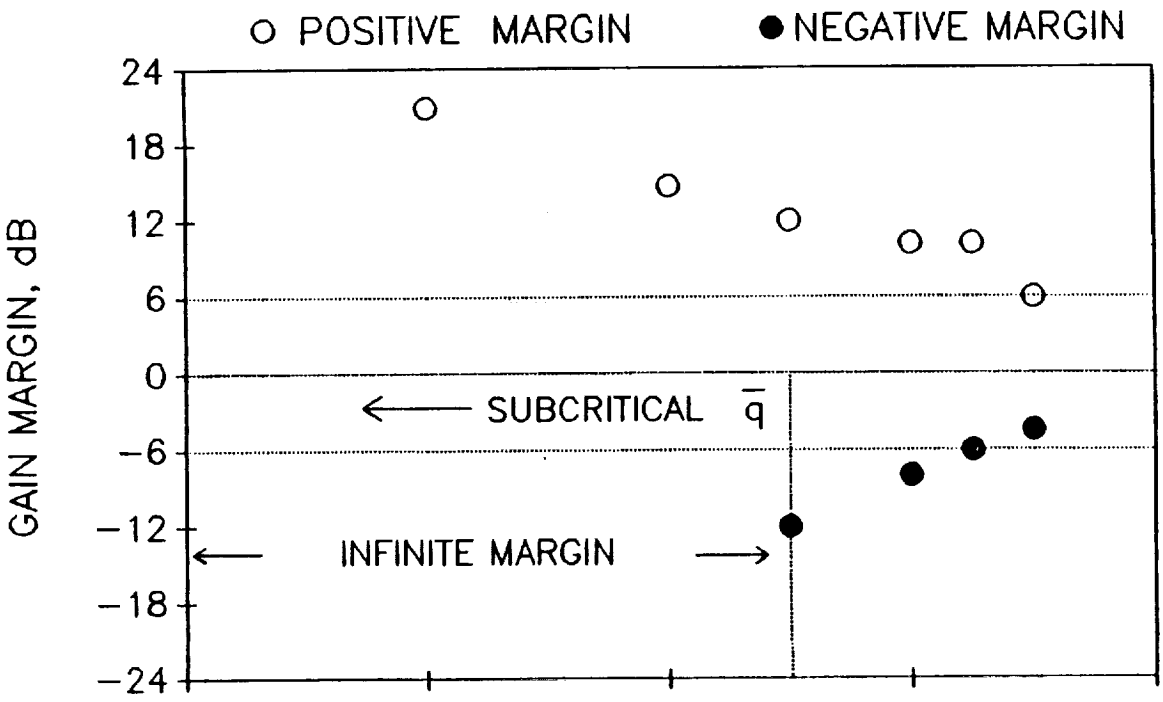


Figure 16a ACSL simulation stability margins – gain margin.

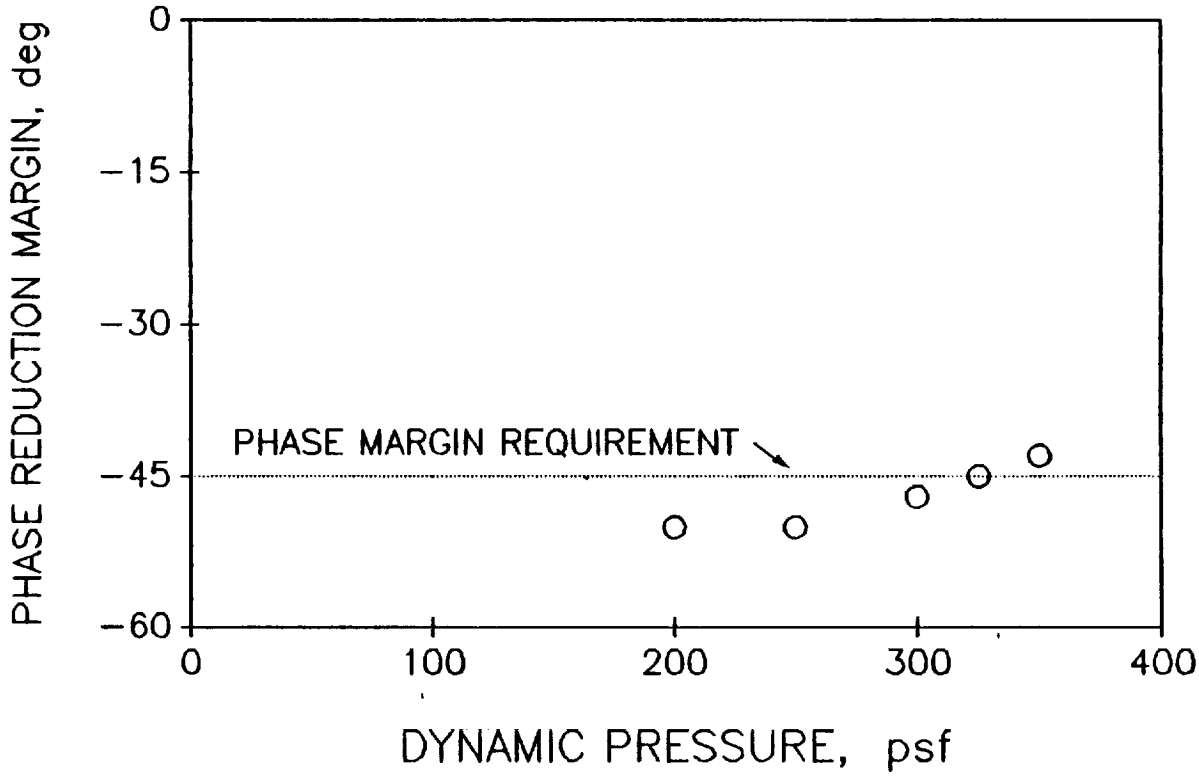


Figure 16b ACSL simulation stability margins – phase margin.

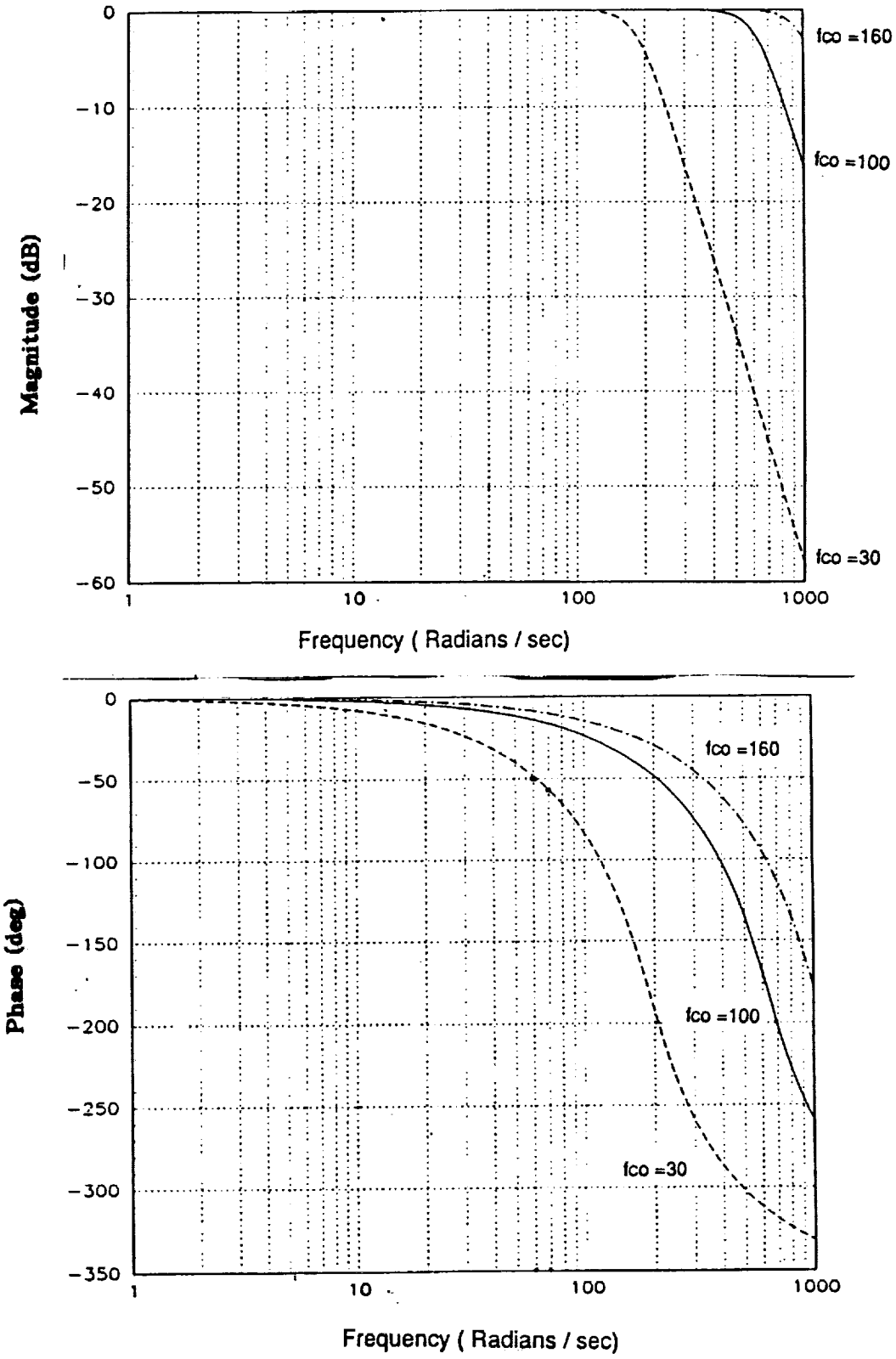


Figure 17 Butterworth filter characteristics parameterized by fco in Hz.

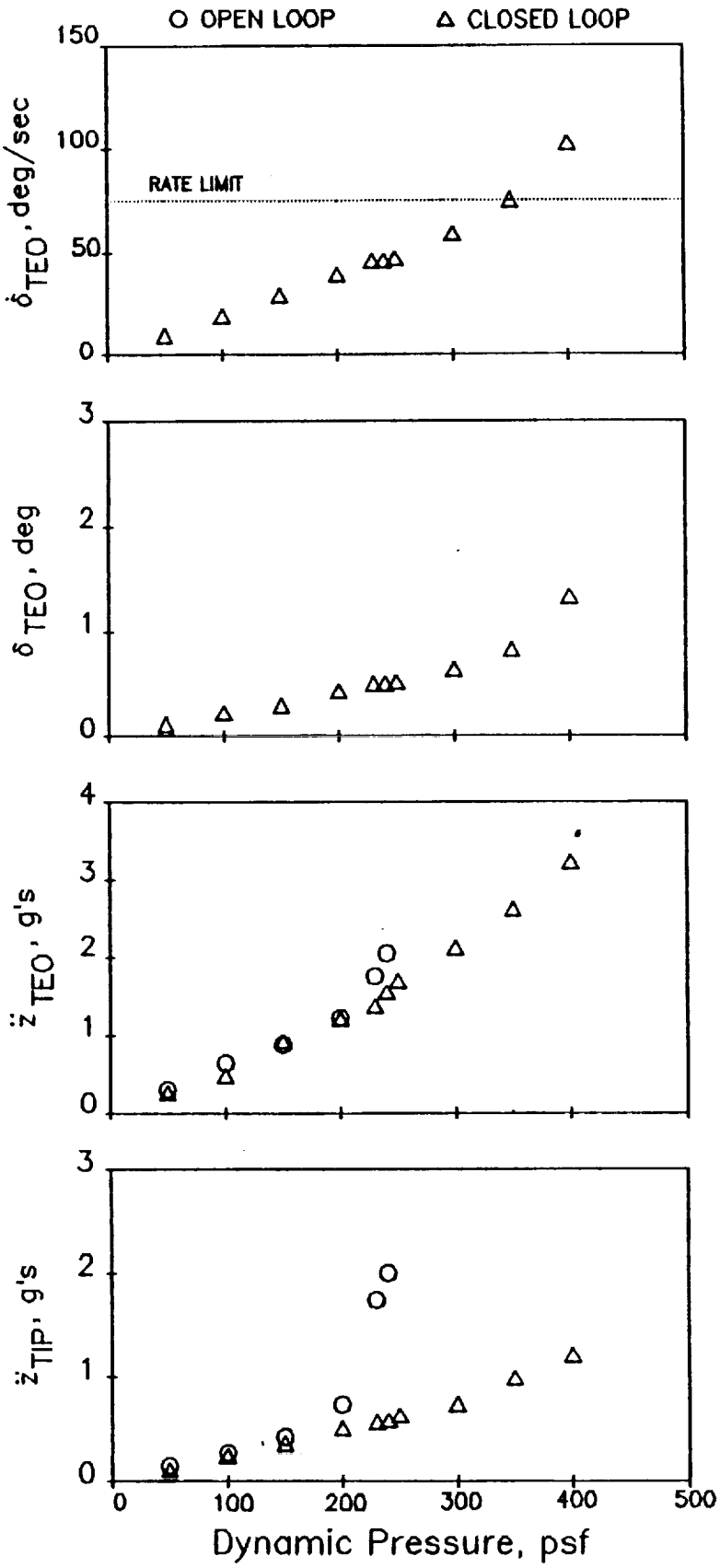


Figure 18 ACSL simulation RMS response summary
(1 foot/sec RMS gust input).

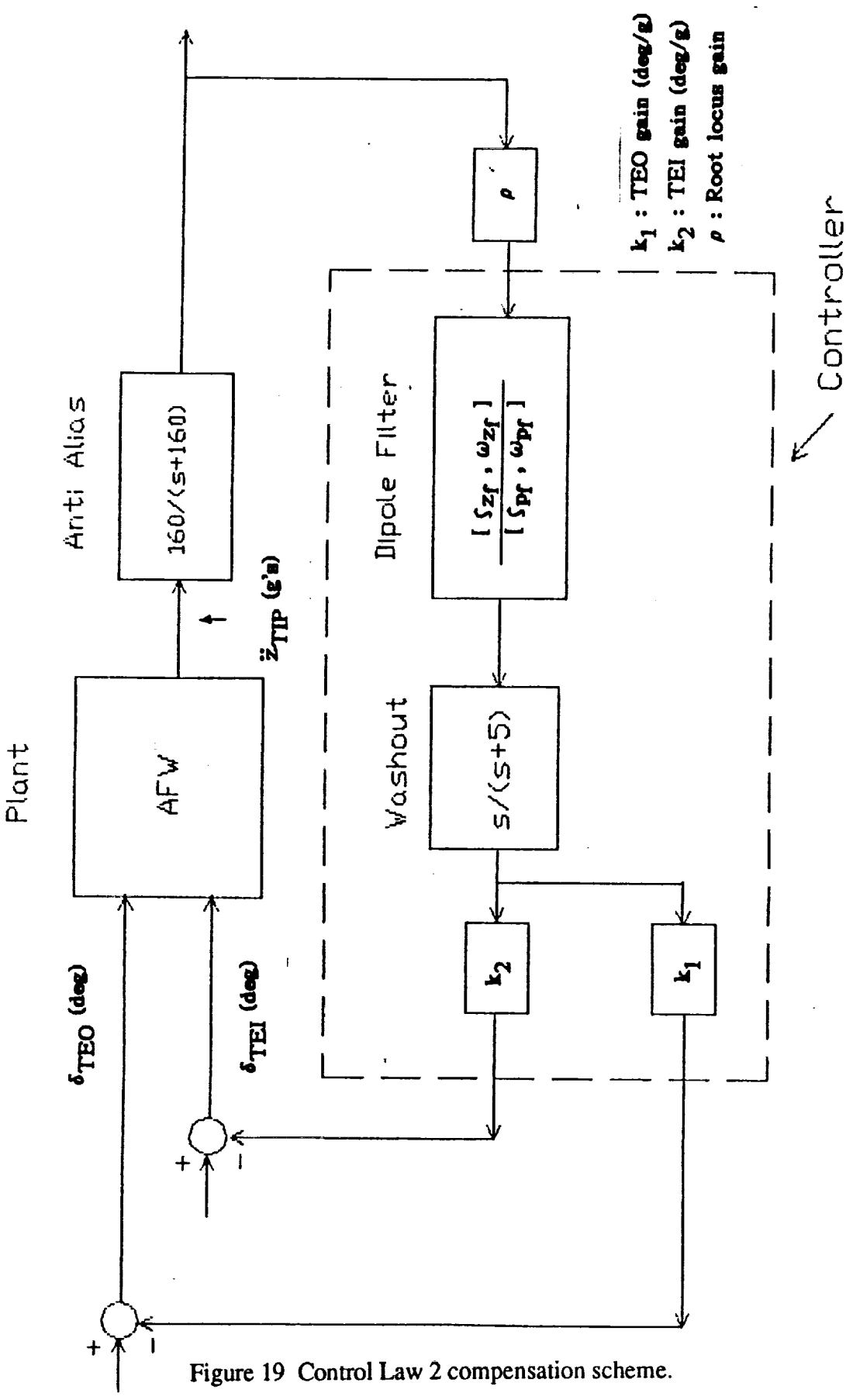


Figure 19 Control Law 2 compensation scheme.

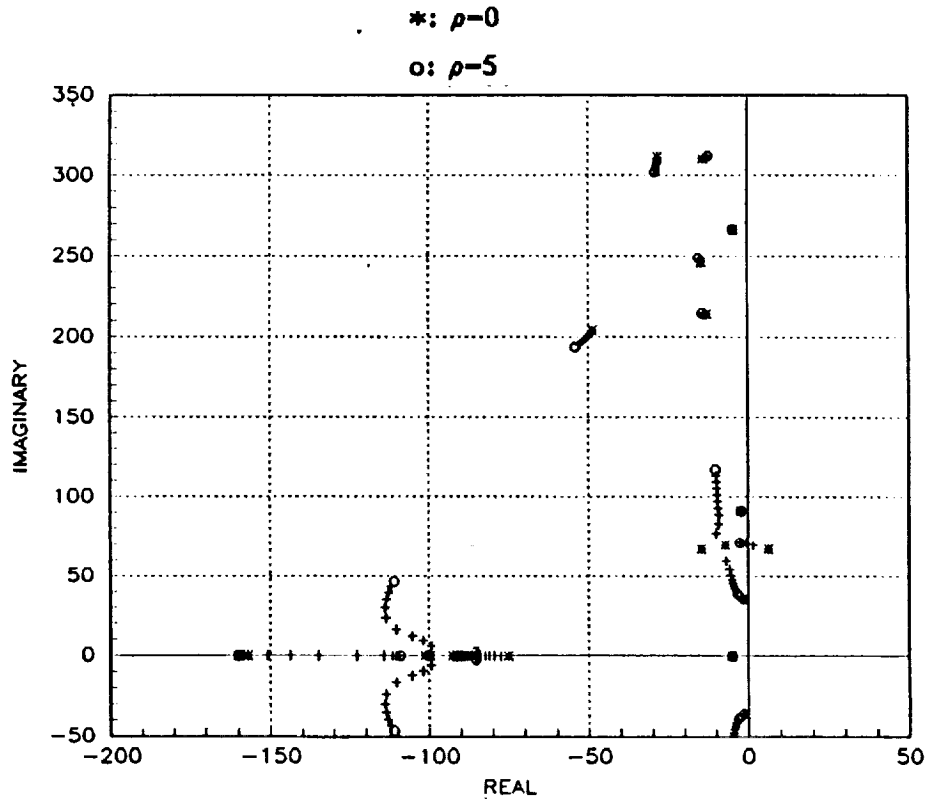


Figure 20a Control Law 2 gain root locus - complete ($k_1 = 0.11$ deg/g ; $|k_2 / k_1| = 0.5$).

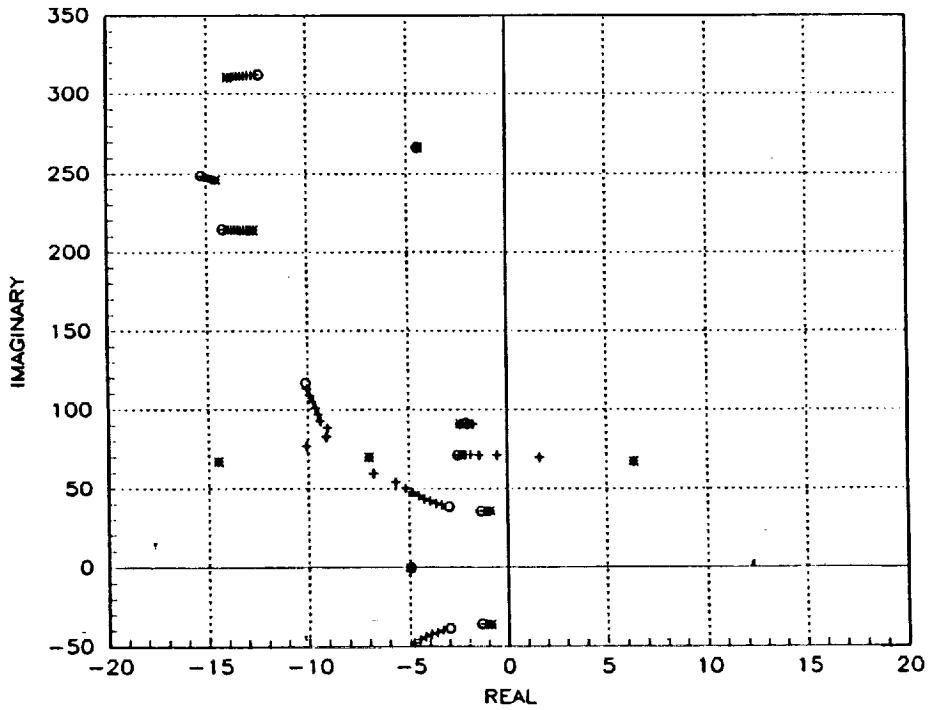


Figure 20b Control Law 2 gain root locus - expanded ($k_1 = 0.11$ deg/g ; $|k_2 / k_1| = 0.5$).

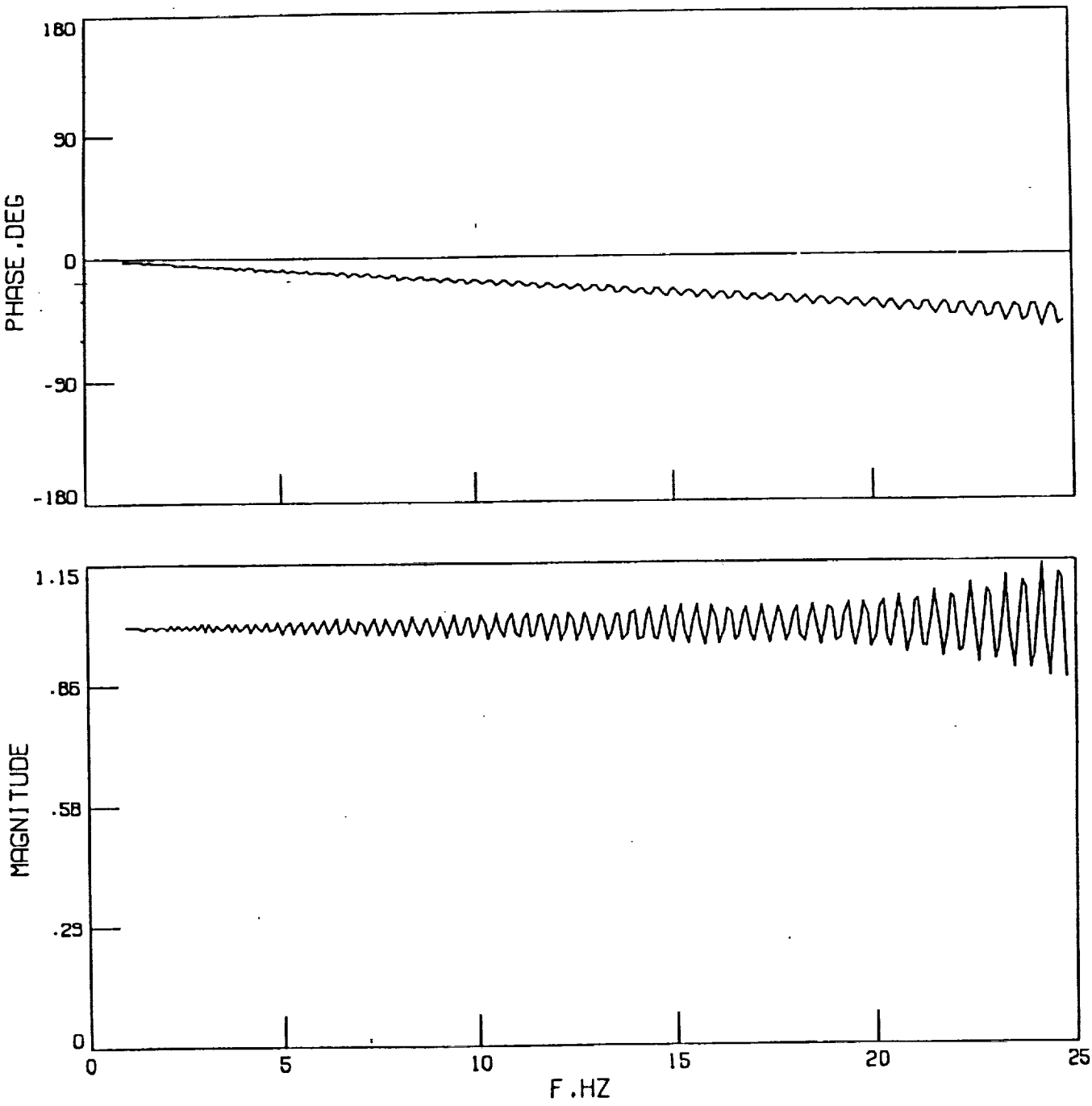


Figure 21 AFW control computer delay characteristics from Hot Bench simulation.

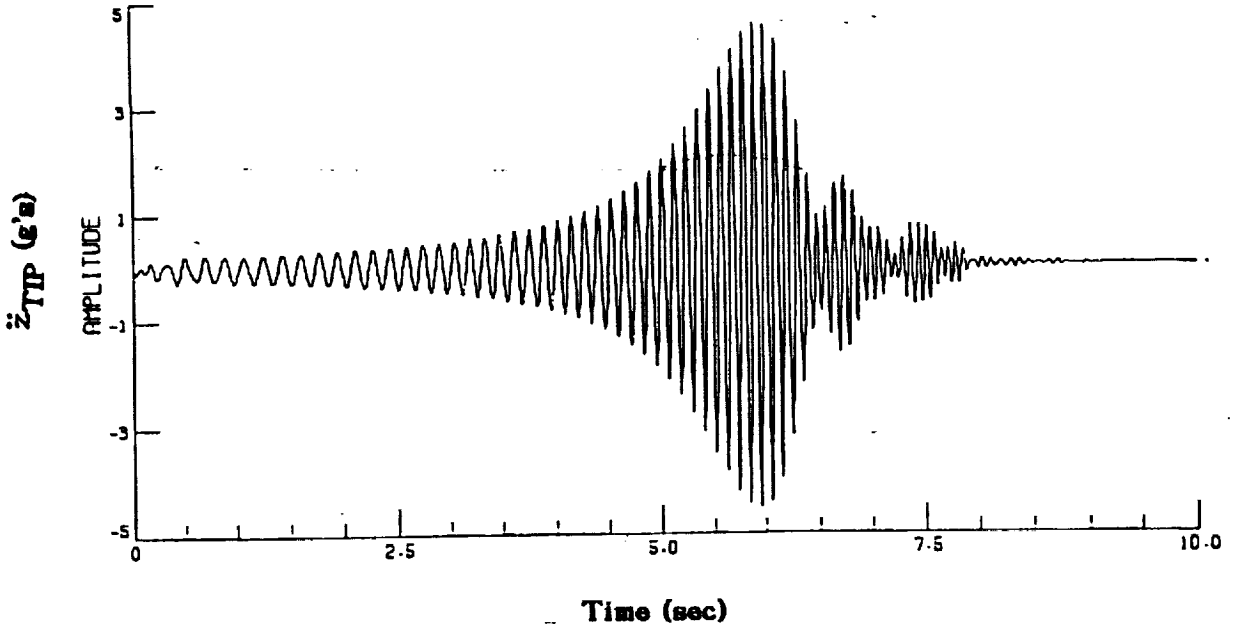


Figure 22a Sine sweep response from Hot Bench simulation – open-loop ($\bar{q}$ = 200 psf).

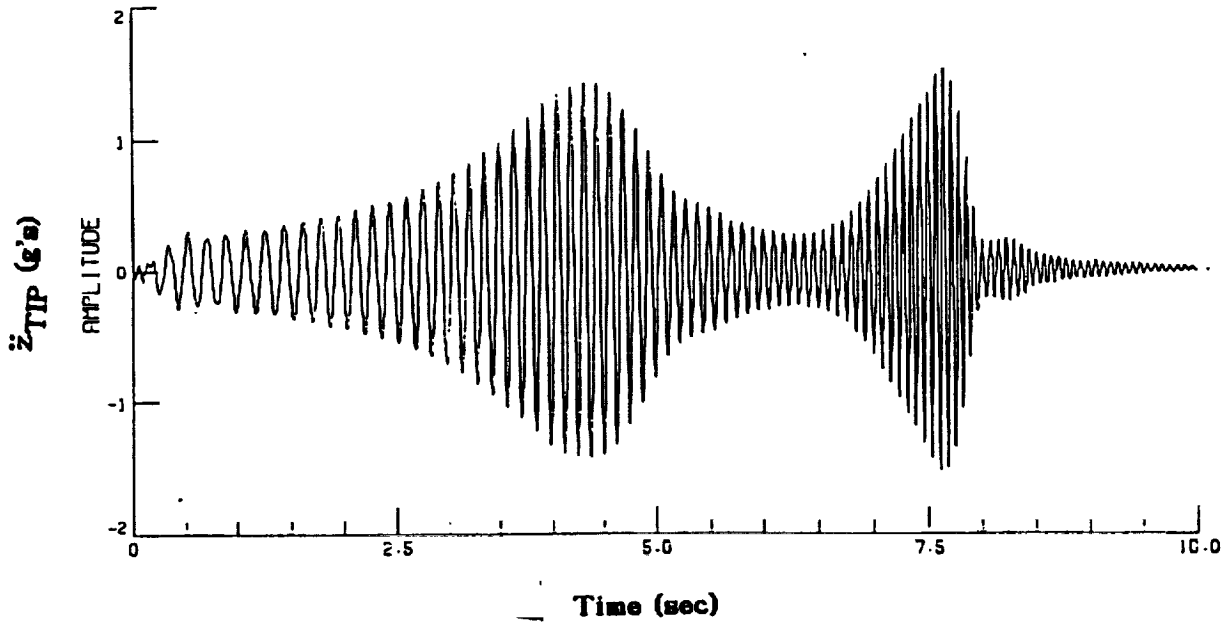


Figure 22b Sine sweep response from Hot Bench simulation – closed-loop ($\bar{q}$ = 200 psf ; k = 0.11 deg/g).

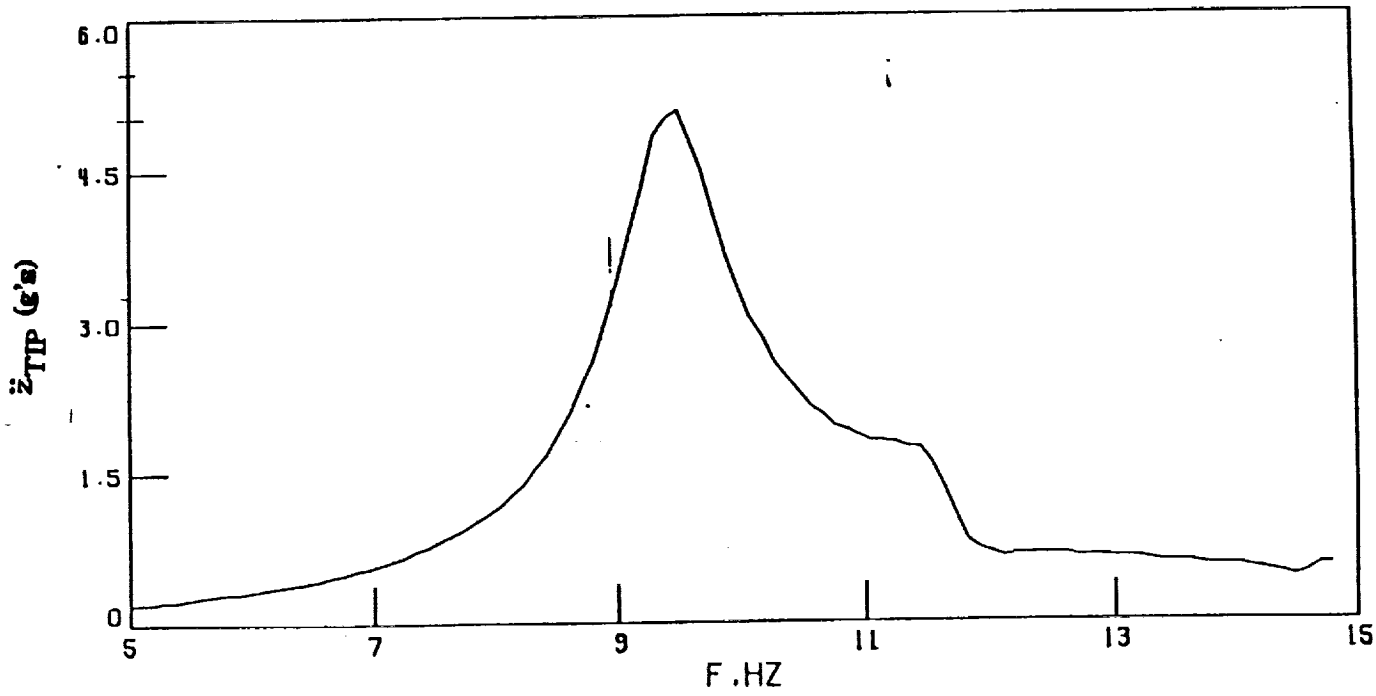


Figure 23a Frequency response magnitude from Hot Bench simulation – open-loop ($\bar{q}$ = 200 psf).

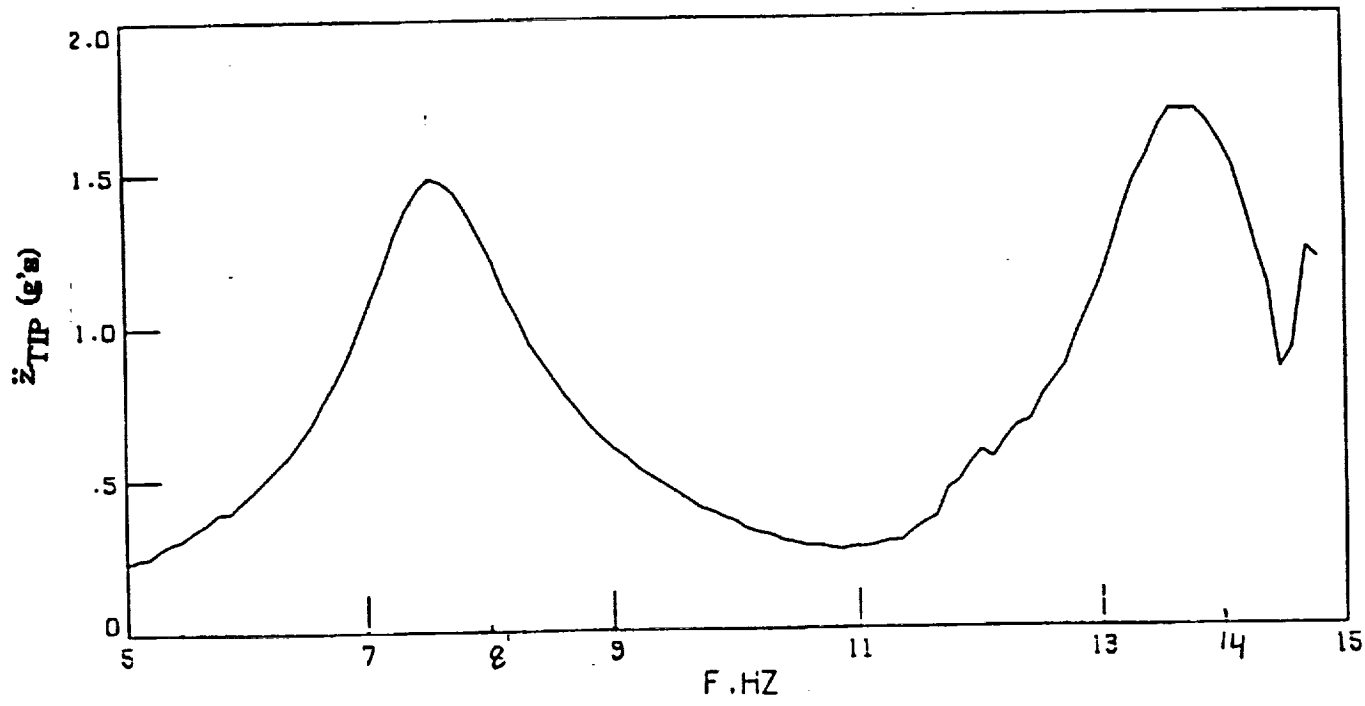


Figure 23b Frequency response magnitude from Hot Bench simulation – closed-loop ($\bar{q}$ = 200 psf ; k = 0.11 deg/g).

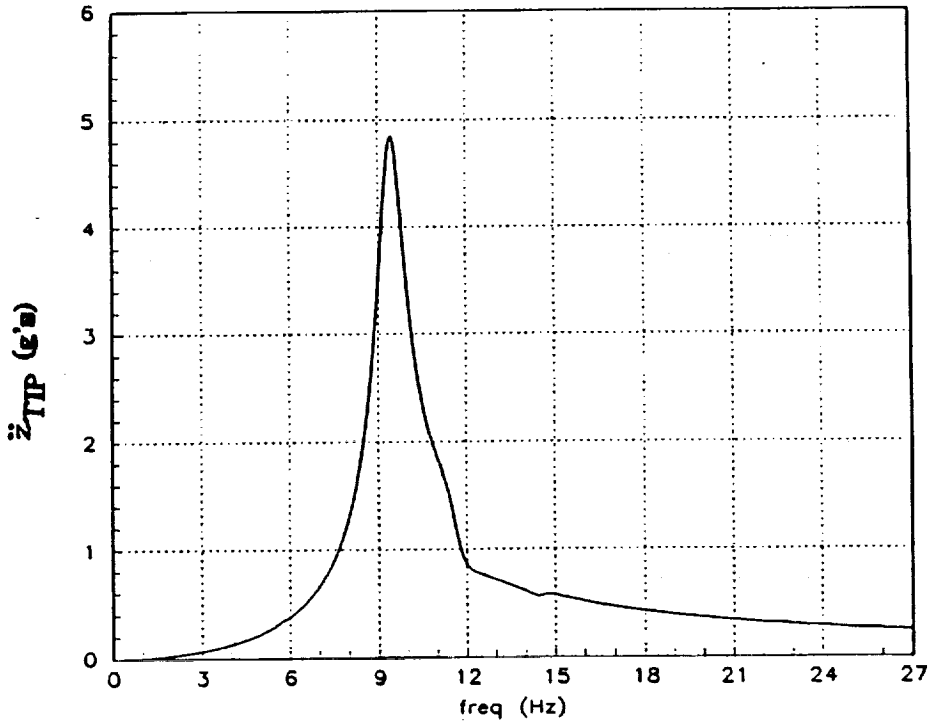


Figure 24a Frequency response magnitude from linear simulation – open-loop ($\overline{q}$ = 200 psf).

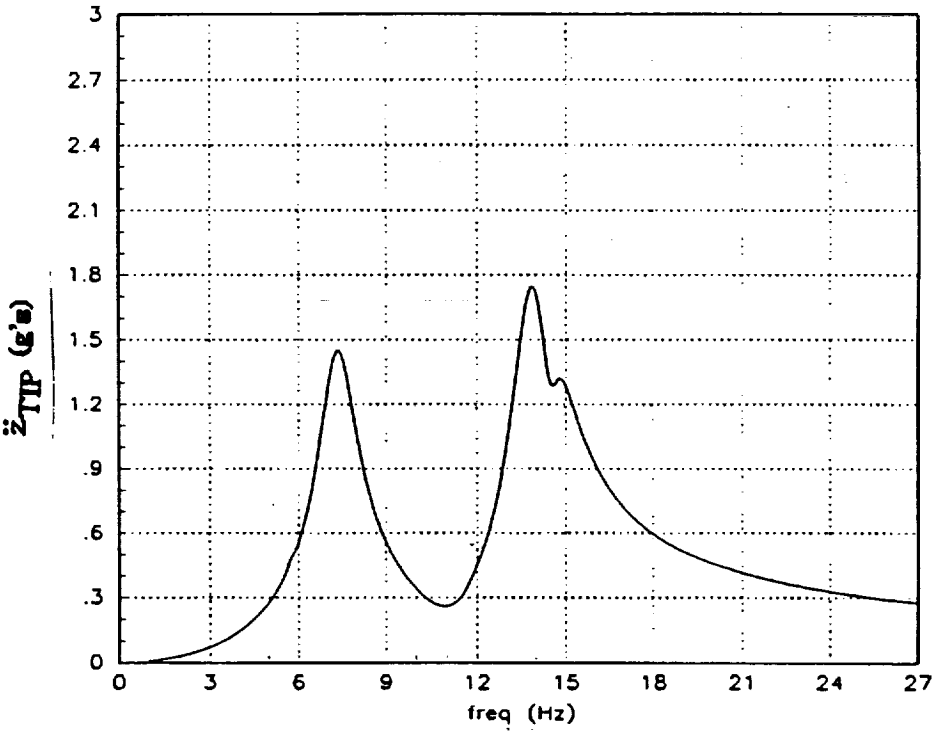


Figure 24b Frequency response magnitude from linear simulation – closed-loop ($\overline{q}$ = 200 psf ; k = 0.11 deg/g).

# REPORT DOCUMENTATION PAGE

*Form Approved*
*OMB No. 0704-0188*



| 1. AGENCY USE ONLY *(Leave blank)* | 2. REPORT DATE | 3. REPORT TYPE AND DATES COVERED |
|---|---|---|
| | September 1992 | Technical Memorandum |

**4. TITLE AND SUBTITLE**
Active Flutter Suppression Using "Dipole" Filters

**5. FUNDING NUMBERS**
505-64-52-03

**6. AUTHOR(S)**
S. Srinathkumar and Martin R. Waszak

**7. PERFORMING ORGANIZATION NAME(S) AND ADDRESS(ES)**
NASA Langely Research Center
Hampton, VA 23681-0001

**8. PERFORMING ORGANIZATION REPORT NUMBER**

**9. SPONSORING / MONITORING AGENCY NAME(S) AND ADDRESS(ES)**
National Aeronautics and Space Administration
Washington, DC 20546-0001

**10. SPONSORING / MONITORING AGENCY REPORT NUMBER**
NASA TM-107594

**11. SUPPLEMENTARY NOTES**
Srinathkumar: National Aeronautical Laboratory, Bangalore, India; and Waszak: Langley Research Center, Hampton, VA

**12a. DISTRIBUTION / AVAILABILITY STATEMENT**
Unclassified-Unlimited

Subject Category 08

**12b. DISTRIBUTION CODE**

**13. ABSTRACT** ***(Maximum 200 words)***

By using traditional control concepts of gain root locus, the active suppression of a flutter mode of a flexible wing is examined. It is shown that the attraction of the unstable mode towards a critical system zero determines the degree to which the flutter mode can be stabilized. For control situations where the critical zero is adversely placed in the complex plane, a novel compensation scheme called a 'Dipole' filter is proposed. This filter ensures that the flutter mode is stabilized with acceptable control energy. The control strategy is illustrated by designing flutter suppression laws for an active flexible wing (AFW) wind-tunnel model, where minimal control effort solutions are mandated by control rate saturation problems caused by wind-tunnel turbulence.

**14. SUBJECT TERMS**
control system design, flutter suppression, aeroelasticity, active control

**15. NUMBER OF PAGES**
40

**16. PRICE CODE**
A03

| 17. SECURITY CLASSIFICATION OF REPORT | 18. SECURITY CLASSIFICATION OF THIS PAGE | 19. SECURITY CLASSIFICATION OF ABSTRACT | 20. LIMITATION OF ABSTRACT |
|---|---|---|---|
| Unclassified | Unclassified | | |